Spectroscopic analysis of 8-hydroxyquinoline-5-sulphonic acid and investigation of its reactive properties by DFT and molecular dynamics simulations

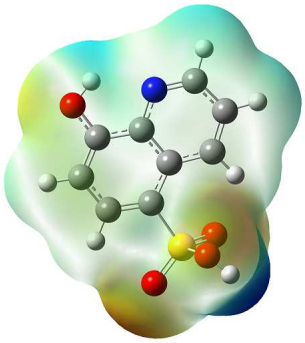

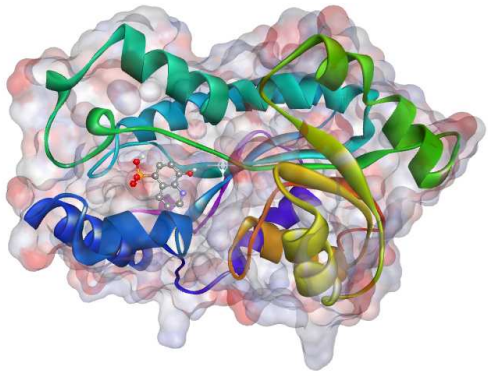

Spectroscopic analysis of 8-hydroxyquinoline-5-sulphonic acid and investigation of its reactive properties by DFT and molecular dynamics simulations

Sureshkumar B[a], Sheena Mary Y[b*], C.Yohannan Panicker[b], K.S.Resmi[b], Suma.S[a], Stevan Armaković[c], Sanja J. Armaković[d], C.Van Alsenoy[e]

[a]Department of Chemistry, SN College, Kollam, Kerala, India

[b]Department of Physics, Fatima Mata National College, Kollam, Kerala, India

[c]University of Novi Sad, Faculty of Sciences, Department of Physics, Trg D. Obradovića 4, 21000 Novi Sad, Serbia

[d]University of Novi Sad, Faculty of Sciences, Department of Chemistry, Biochemistry and Environmental Protection, Trg D. Obradovića 3, 21000 Novi Sad, Serbia

[e]Department of Chemistry, University of Antwerp, Groenenborgerlaan 171, B-2020, Antwerp, Belgium

*author for correspondence: email: sypanicker@rediffmail.com

Abstract

A detailed interpretation of the FT-IR and FT-Raman spectra has been performed on the basis of the observed and calculated infrared and Raman spectra as well as calculated potential energy distribution values. Comparison of Raman and SERS spectra suggests a tilted orientation of the rings on the metal surface. The dipole moment, polarizability and first and second order hyperpolarizability values of the molecule were calculated. Global reactivity parameters were predicted. The relative reactivities towards electrophilic and nucleophilic attack are predicted using molecular electrostatic potential map. Average local ionization energy (ALIE) and Fukui functions have been inspected in order to investigate local reactivity properties of title molecule. The importance of autoxidation and hydrolysis mechanisms for the title molecule has been assessed by DFT calculations of bond dissociation energies (BDE) and by calculations of radial distribution functions (RDFs) after molecular dynamics (MD) simulations. Molecular docking studies suggest that the title compound can be a lead compound for developing new anti-cancerous drug.

Keywords: DFT; Quinoline; SERS; ALIE; RDF; Molecular docking.

1. Introduction

8-hydroxyquinoline and its derivatives have wide applications in various fields, light emitting diodes [1], nuclear medicine [2], treating cancer [3] and neurodegenerative disorder

[4]. The luminescence properties of 8-hydroxyquinoline complexes are widely used for the detection and quantification of metal ions [5-7] and for the selective metal ion determination by use of time resolved measurements [8]. Vitali et al. [9] was developed a novel carbon paste electrode containing chitosan cross linked with the chelating agent 8-hydroxyquinoline-5-sulphonic acid and glutaraldehyde for the determination of Cu(II). Substituted sulphonic acid is used as analytical reagent in the manufacture of disinfectants, deodorants, antiseptics, medicines, for the treatment of minor wounds, for disinfecting skin and purification of drinking water in case of amoebicidal and bactericidal emergencies. Recently a number of vibrational, DFT computational and molecular docking studies of quinoline derivatives are reported in literature [10-16]. Since title molecule is a candidate to be used as an active component of some future pharmaceutical product we decided to investigate its local reactivity properties from the ecological aspect. Namely, molecules with possibly important biological activities are very stable in aquatic mediums, leading to their accumulation [17]. So far such organic compounds have been detected in all types of water and what is of great concern is that conventional water purification methods are not efficient enough to remove them [18,19]. To properly treat the waste waters it is proposed to use advanced oxidation procedures [18, 20-25]. Procedures based on advanced oxidation processes are rather complicated because different pharmaceutical molecules have different reactive properties. In order to predict reactive properties of organic molecules the principles of molecular modeling are frequently applied [26-29], in such way optimizing and rationalizing the experimental procedures related to degradation of pharmaceutical pollutants. It is well established that autoxidation mechanism is closely related with the bond dissociation energies for hydrogen abstraction, which are readily calculated within DFT approach. On the other side the influence of solvent (water) can be assessed by calculations of radial distribution functions (RDF) after molecular dynamics (MD) simulations. In the present work, the vibrational spectroscopic analysis of 8-hydroxy quinoline- 5-sulphonic acid (8HQ5SA), SERS study, molecular dynamics and molecular docking studies are reported.

2. Experimental details

A fine sample of 8HQ5SA was obtained from Sigma Aldrich chemical company, USA and used without any further purification for spectral measurements. The FT-IR spectrum (Fig.1) of 8HQ5SA was recorded in the region 4000-400 cm^{-1} using Perkin-Elmer spectrum RX1 spectrometer equipped with Helium-Neon laser source, potassium bromide beam splitter and LiTaO3 detector. The sample was prepared by pressing 8HQ5SA with KBr into pellet form. The FT-Raman spectrum (Fig.2) of 8HQ5SA was recorded in 4000-0 cm^{-1} with a Nocolet

model 950 FT-Raman spectrometer at 4 cm^{-1} spectral resolution using the 1064 nm line of a Nd:YAG laser for excitation at a 200 mW output power. The silver colloid was prepared by the reported protocol in literature [30, 31] and aged for two weeks before being used for the SERS analysis. The solutions were prepared with distilled, deionized water and SERS samples as reported in literature [32]. The SERS spectrum (Fig.3) was carried in aplha500RA confocal Raman microscope using 488 nm.

3. Computational details

DFT calculations of 8HQ5SA were performed using Gaussian 09 software package [33] at B3LYP functional combined with aug-CC-pVDZ (5D, 7F) basis set to obtain the optimized geometry (Fig.4). The theoretically obtained wavenumbers are scaled by a scaling factor of 0.9613 [34] and the vibrational assignments are done by Gaussview program [35] and with the help of potential energy distribution [36]. In this work we have used Jaguar 9.0 program [37] for DFT calculations of ALIE, Fukui functions and BDEs with B3LYP exchange-correlation functional [38-42] and with 6-311++G(d,p), 6-31+G(d,p) and 6-311G(d,p) basis sets, respectively. For MD simulations Desmond [39] program has been used with OPLS 2005 force field [43] within isothermal–isobaric (NPT) ensemble class. Other important MD parameters include simulation time set to 10 ns, temperature to 300 K, pressure to 1.0325 bar and cut off radius to 12 Å. Modeled system was created by placing of one 8HQ5SA molecule into the cubic box with ~3000 molecules with simple point charge (SPC) model [44] used for the theoretical treatment of solvent. Thanks to the method of Johnson et al. [45, 46], implemented into the Jaguar program, the analysis of electron density was conducted in order to determine intramolecular noncovalent interactions. Maestro GUI [47] was used for the preparation of input files and analysis of results obtained with Jaguar and Desmond programs. Maestro, Jaguar and Desmond programs were used as implemented in Schrödinger Materials Science Suite 2015-4.

4. Results and discussion

In the present discussion, the rings, C_3-C_4-C_9-C_{11}-C_{12}-C_8 and C_1-C_2-C_3-C_4-N_{15}-C_5 are designated as PhI and PhII, respectively.

4.1 Geometrical parameters

The optimized geometrical parameters of 8HQ5SA are given in table 1. The C_9-C_{11} bond length of 8HQ5SA is 1.3811Å which is less than that of C_9-C_4 (1.4360 Å) because of the delocalization of electrons due to the presence of C-OH group. Also the bond length of C_8-C_{12} (1.3838 Å) is less than that of C_8-C_3 (1.4300 Å) owing to the delocalization of electrons. The large value of the bond length of C_4-C_3 (1.4260 Å) is due to the delocalization

of electron density due to the adjacent quinoline ring. The C_4-N_{15} and C_5-N_{15} bond lengths of 8HQ5SA are respectively, 1.3586 Å and 1.3202 Å while the reported values for similar derivatives are 1.3874 Å and 1.3345 Å [48] and 1.3662 Å and 1.3202 Å [49] and 1.3626 Å and 1.3187 Å [50]. For 8HQ5SA, the S=O bond lengths are, 1.4846 Å and 1.4786 Å and the reported values are 1.4613, 1.4564 Å [50], 1.4660, 1.4620 Å [48] and 1.4721, 1.4551 Å [49]. The reported value of the C-S bond length is 1.7770 Å [48], 1.7562 Å [49] and 1.7754 Å [50] and in the present case the corresponding C-S bond length is 1.7873 Å. The OSO and OSC bond angles of 8HQ5SA are, 119.5, 106.6, 108.5° and 112.1, 109.7° respectively while the reported values are 113.6, 111.9, 113.2° (OSO), 105.2, 106.5, 105.8° (OSC) [48] and 109.9, 111.0, 113.9° (OSO), 107.2, 107.7, 107.5° (OSC) [49] and 110.7, 113.2, 111.9° (OSO), 107.3, 107.2, 106.4° (OSC) [50]. The sulfonyl group is tilted from the phenyl ring as is evident from the torsion angles, C_{11}-C_{12}-C_8-S_{18} = -179.5°, C_{12}-C_8-S_{18}-O_{21} = -108.8°, C_4-C_3-S_8-S_{18} = 179.9° and C_3-C_8-S_{18}-O_{21} = 71.4°.

4.2 IR and Raman spectra

The wavenumbers (calculated scaled, observed IR and Raman) and vibrational assignments of 8HQ5SA are presented in table 2. For 8HQ5SA, the bending modes (in-plane and out-of-plane) of the OH is assigned at 1400 cm^{-1} and at 671 cm^{-1} theoretically with PEDs 39 and 84%, which are expected in the ranges 1400 ± 40 cm^{-1} and 650 ± 80 cm^{-1} [51, 52]. These modes have IR intensities, 14.11 and 79.56 and Raman intensities, 100.97 and 1.39. Experimentally bands are seen in the Raman spectrum at 1408 and 677 cm^{-1}. The C-O stretching mode is assigned at 1260 cm^{-1} in the Raman spectrum and at 1255 cm^{-1} theoretically with IR intensity, 114.67, Raman activity, 15.16 and PED value of 36% and according to literature, this vibration is in the region 1220 ± 40 cm^{-1} [51-53]. The reported values of C-O stretching and OH out-of-plane deformations are respectively, 1257 cm^{-1} and 665 cm^{-1} (DFT), 653 cm^{-1} (IR), 667 cm^{-1} (Raman) [54].

For 8HQ5SA, the SO_2 stretching vibrations are assigned at 1213 and 1030 cm^{-1} theoretically which are expected in the range 1300-1000 cm^{-1} [51] and experimentally bands are observed at 1035 cm^{-1} in the IR spectrum and at 1217, 1035 cm^{-1} in the Raman spectrum. The Raman activities of these modes are 7.26 and 8.50 while the IR intensities are high, 166.25 and 75.87 with PEDs 78 and 62%. The reported values of SO_2 stretching modes are at 1262, 1052 cm^{-1} [55] and at 1306, 1114 cm^{-1} by Sebastian et al. [56]. The deformation modes of the SO_2 moiety are in the regions, 560 ± 40 cm^{-1} (scissoring), 550 ± 55 cm^{-1} (wagging), 440 ± 50 cm^{-1} (twisting) and the rocking mode at around 350 cm^{-1} [51]. For 8HQ5SA, the SO_2 deformation modes are assigned at 493, 450, 406, 357, 267 cm^{-1}

theoretically. Experimentally bands are observed at 452 cm^{-1} in the IR spectrum and at 404, 358, 267 cm^{-1} in the Raman spectrum. The Raman activities of these modes are less than 10 while these modes possess average IR intensities with PEDs ranging from 61 to 38%. The SO_2 deformations are reported at 569, 518, 388 cm^{-1} in IR, 514 cm^{-1} in Raman, 569, 511, 408, 388 cm^{-1} (DFT) [57]. By comparison with SOH bending wavenumbers in sulfuric acid and other sulphonic acids, the band at 1187 cm^{-1} is assigned to SOH bend of 8HQ5SA [58, 59]. Experimentally bands are observed at 1190 cm^{-1} in the IR spectrum and at 1185 cm^{-1} in the Raman spectrum as this SOH bending mode. For 8HQ5SA, the C-S stretching mode is observed at 633 cm^{-1} in the IR spectrum and the band at 633 cm^{-1} (DFT) with PED 33% is assigned as this mode [51]. The reported values of C-S stretching modes are 632 cm^{-1} (Raman), 639 cm^{-1} (DFT) [60] and at 661 cm^{-1} (IR), 653 cm^{-1} (Raman), 664 cm^{-1} (DFT) [57].

In poly substituted benzenes, the aromatic CH stretching modes [53] absorb weakly to moderately between 3000 and 3120 cm^{-1} and in the present case, the modes at 3097 and 3085 cm^{-1} (DFT) are assigned the CH stretching modes of the phenyl ring [61]. The ring stretching modes of the phenyl ring PhI are assigned at 1601, 1544, 1476, 1436, 1334 cm^{-1} theoretically and at 1602, 1550, 1482, 1429 cm^{-1} in the IR spectrum and at 1603, 1547, 1472, 1324 cm^{-1} in the Raman spectrum, experimentally [51]. All these modes have high IR intensities and Raman activities are high only for the modes at 1544, 1476 and 1334 cm^{-1} and the PEDs are in the range 40 to 52%. For 8HQ5SA, DFT calculations give the ring breathing mode of the poly substituted phenyl ring at 1017 cm^{-1} with a PED of 42%. The ring breathing mode for poly substituted benzene ring is reported at 1006 cm^{-1} in the IR spectrum and at 998 cm^{-1} theoretically [62] and at 1003 cm^{-1} theoretically [61]. In the present case, the bands at 1169, 1093 cm^{-1} (IR), 1170, 1094 cm^{-1} (Raman), 1172, 1098 cm^{-1} (DFT) and 953, 851 cm^{-1} (IR), 957, 840 cm^{-1} (Raman), 954, 845 cm^{-1} (DFT) are assigned as the in-plane and out-of-plane CH deformations of the poly-substituted phenyl ring. According to literature [63], for tetra-substituted benzenes, a strong band is seen in 850-840 cm^{-1} due to out-of-plane CH deformation and in the present case this mode appears at 845 cm^{-1}. The ring PhII modes are assigned at 3115, 3076, 3025 cm^{-1} (IR), 3109, 3077 cm^{-1} (Raman), 3107, 3078, 3044 cm^{-1} (DFT) (CH stretching modes), 1571 cm^{-1} (DFT) (C=C stretching) mode, 1055 cm^{-1} (IR), 908 cm^{-1} (Raman), 1052, 915 cm^{-1} (DFT) (C-C stretching modes), 1233 cm^{-1} (IR), 1260 cm^{-1} (Raman), 1255, 1237 cm^{-1} (DFT) (C-N stretching modes), 1372, 1130 cm^{-1} (IR), 1372, 1130 cm^{-1} (Raman), 1368, 1349, 1127 cm^{-1} (DFT) (in-plane CH deformation modes) and at 972, 779 cm^{-1} (IR), 977, 782 cm^{-1} (Raman), 970, 935, 781 cm^{-1} (DFT) (out-of-plane CH

deformation modes) [51] and these assignments are in agreement with reported values [15,16].

4.3 SERS spectrum

Raman scattering efficiency can be increased by many orders of magnitude if the analyte is situated on the surface of a noble metal and this amplification of surface-enhanced Raman scattering has found application in the tracking of drug delivery systems. 8HQ5SA has a number of potential adsorption sites for the possible interactions with the metal surfaces; the lone pair of electrons in the oxygen atoms and π-electrons of the rings. SERS has been used to study the adsorption mechanism of molecule adsorbed onto the surface of coinage metals [64, 65] and the SERS spectrum is analyzed based of the SERS wavenumbers and relative change in the intensities of SERS and normal Raman bands [66-68]. According to surface selection rules of SERS, for a molecule adsorbed flat on a metal surface, its out-of-plane modes will be more enhanced when compared with the in-plane modes and vice versa when it is adsorbed perpendicular to the surface [69]. Also the vibrations involving atoms that are close to the metal surface will be enhanced. When the shift between the normal Raman and SERS bands are greater than 5 cm^{-1}, there is a flat orientation to the metal surface [69, 70].

For the ring PhI, the ring stretching modes are observed in the SERS spectrum at 1628, 1528, 1481, 1430 and 1328 cm^{-1}. The modes 1628, 1481 and 1328 cm^{-1} are up shifted by 25, 9 and 4 cm^{-1} while the mode 1528 cm^{-1} in SERS is down shifted by 19 cm^{-1} from the normal Raman spectrum. Corresponding to the SERS band at 1430 cm^{-1}, no band is observed in the normal Raman spectrum. These changes in the ring stretching modes should correspond to a tilted or perpendicular orientation according to the SERS selection rules [71, 72] and the wavenumber shift was associated with a probable charge transfer between the molecule with the metal surface as reported in literature [73].

The ring stretching vibrations of PhII are present in the SERS spectrum at 1565, 1280, 1240 and at 1055 cm^{-1} and in the normal Raman spectrum only one mode is present at 1260 cm^{-1}. Most of these modes possess high intensity and substantial band broadening, which indicate somewhat flat orientation on the metal surface as reported in literature [74]. The substantial shifts observed for the ring modes could also be attributed to interaction of the π-electrons with the surface. The presence or absence of the phenyl ring CH stretching mode is a reliable probe for the perpendicular or parallel orientation, respectively, of the phenyl ring with respect to the metal surface, since CH stretching modes do not mix significant with other vibrational modes of the aromatic rings [69, 70].

In the present case, CH stretching modes are present in the SERS spectrum at 3087 cm^{-1} which is absent in the normal Raman spectrum for PhI and at 3120 cm^{-1} for the ring PhII. The in-plane CH deformation modes of the phenyl ring PhI are present in the SERS spectrum at 1178 and 1105 cm^{-1} while the normal Raman modes are at 1170 and 1094 cm^{-1}. Also the out-of-plane CH deformation modes are present in the SERS spectrum at 835 cm^{-1} for PhI ring and at 980 cm^{-1} for PhII. The presence of in-plane and out-of-plane CH modes for the ring PhI in the SERS spectrum suggests a tilted orientation for PhI while the presence of out-of-plane mode of PhII suggests a flat orientation as reported in literature [69, 70]. Also the ring deformation modes are present in the SERS spectrum at 605, 177 cm^{-1} for PhI and at 560, 470, 177 cm^{-1} for PhII rings and the presence of these modes suggest tilted orientation for the rings [74].

The SO_2 and SO stretching modes are present in the SERS spectrum at 1212 cm^{-1} and 701 cm^{-1} and this indicates that the sulpho group is probably near to the metal surface. Also the presence of SERS bands at 701, 510, 365, 309 and 220 cm^{-1} corresponding to SO_2 deformation modes support the possibility of direct interaction between the sulpho group and the metal surface. According to SERS studies, this is justifiable because the modes of groups directly interacting with the metal surface will be prominent in the SERS spectrum with a wavenumber shift [75]. The normal Raman band at 1408 cm^{-1} is the in-plane OH deformation and the corresponding SERS band is at 1395 cm^{-1} and this shift suggest a tilted orientation of COH moiety which is supported by the modes at 1280 and 309 cm^{-1} in the SERS spectrum (C-O stretch and OH deformation modes) as reported in literature [76]. The presence sulpho and hydroxyl modes in the SERS spectrum suggest that the interaction between PhI is more than the interaction of PhII with the metal as reported in literature [69, 70].

4.4 Nonlinear optical properties

Nonlinear optical effect arise from the interactions of electromagnetic fields in various media to produce new fields altered in phase, frequency, amplitude or other propagation characteristics from the incident fields [77]. NLO properties like the dipole moment, polarizability, first and second order hyperpolarizabilities are calculated using B3LYP/6-311++G(d) (5D, 7F). The total molecular dipole moment of 8HQ5SA is 3.71 Debye, polarizability is 2.291×10^{-23} e.s.u, and the first and second order hyperpolarizabilities are 3.601×10^{-30} and -6.961×10^{-37} e.s.u. Here, the first hyperpolarizability of 8HQ5SA is 27.70 times that of the standard NLO material urea [78] and comparable with the reported values of similar derivatives [57, 79]. The larger component of second order hyperpolarizability is associated with the larger ground state polarization which leads to

strong electronic coupling between the ground and the low lying excited state. Also the NLO properties are related to the energy gap between HOMO and LUMO. The energy gap of 8HQ5SA is 3.119 eV which is lower than that of urea (6.7 eV) [78]. Therefore, the investigated molecule is suitable for nonlinear optical applications.

4.5 Frontier molecular orbital analysis

The frontier orbitals are used to determine the way through which the molecule interacts with other species and the formation of a transition state is due to an interaction between them [80]. The HOMO is related to ionization potential while LUMO is related to electron affinity [81] and the HOMO-LUMO energy gap is a stability index which determines the electron transport properties [82]. In the HOMO-LUMO plot (Fig. 5), the HOMO and LUMO are delocalized over the entire molecule. Using the frontier molecular orbital energies, the ionization potential and electron affinity can be found as: I = -EHOMO, A = -ELUMO [77]. The different chemical descriptors, the hardness (η) and chemical potential (μ) are given by the following relation $\eta = (I-A)/2$ and $\mu = -(I+A)/2$ where I and A are ionization potential and electron affinity [83]. The value of EHOMO = -8.425, ELUMO = -5.306, energy gap = 3.119, global hardness η = 1.5595, chemical potential μ = -6.8655, global electrophilicity index $\omega = \mu^2/2\eta$ = 15.1122 eV in the case of 8HQ5SA. The descriptor, molar refractivity (MR) is an important term used in quantitative structure property relationship and is given as, $MR = 1.333\pi N\alpha$, where N is the Avogadro number and α is the polarizability of the molecular system [84]. For 8HQ5SA, the molar refractivity is 59.65 and this is responsible for the binding property of the molecular system and can be used for the cure of different diseases [85].

4.6 Molecular electrostatic potential

The molecular electrostatic potential (MEP) is related to the electronic density and is a very useful descriptor for determining sites for electrophilic and nucleophilic reactions [81]. The different values of the electrostatic potential are represented by different colors and potential increases in the order of red < orange < yellow < green < blue. In MEP maximum negative region represents the site for electrophilic attack indicated by red color while the maximum positive region represents nucleophilic attack indicated by blue color. As seen from the MEP map (Fig. S1-supporting information) of 8HQ5SA, regions of negative potential are over the electro negative oxygen atoms and the regions having the positive potential are over the hydrogen atoms of the OH groups.

4.7 ALIE surface, Fukui functions and noncovalent interactions

Calculation of the ALIE values offers determination of the molecule areas that are sensitive towards the electrophilic attacks. ALIE provides information on the amount of energy necessary to remove an electron from the investigated molecule. This quantity has been introduced by Sjoberg et al. [86, 87] as a sum of orbital energies weighted by the orbital densities according to the following equation:

$$I(r)=\sum_i \frac{\rho_i(\vec{r})|\varepsilon_i|}{\rho(\vec{r})}, \quad (1)$$

where $\rho_i(\vec{r})$ denotes electronic density of the i-th molecular orbital at the point $\vec{r}$, ε_i denotes orbital energy, while $\rho(\vec{r})$ denotes total electronic density function [88,89]. Where ALIE values are the lowest, electrons are the least tightly bonded and therefore the most easily removed. Such molecule sites are prone to electrophilic attacks. In this work ALIE values are visualized by mapping of its values to the electron density surface, Fig.6. Examination of Fig.6 indicates that 8HQ5SA molecule is the most sensitive towards the electrophilic attacks in the near vicinity of nitrogen atom N15 and carbon atom C12. These molecule sites, designated by the red color in Fig.6, are characterized by ALIE values of ~217 kcal/mol. On the other side the highest ALIE values have been calculated for hydrogen atoms H17 and H22, belonging to OH groups, characterized by ALIE values of ~388 kcal/mol. At these molecule sites the electrons are the most tightly bound and pronounced interactions with water molecules could be expected there. Thanks to the inspection of electron density between the atoms of 8HQ5SA molecule two intramolecular noncovalent bonds have been determined, between N15–H17 and O19–H7, with corresponding strengths of –0.025 and –0.012 electron/bohr^3, respectively.

Determination of other possibly important reactive centers has been performed by calculations of Fukui functions and their mapping to the electron density surface. In Jaguar program the finite difference approach is used for the calculations of Fukui functions according to the following equations:

$$f^+ = \frac{\left(\rho^{N+\delta}(r)-\rho^N(r)\right)}{\delta}, \quad (2)$$

$$f^- = \frac{\left(\rho^{N-\delta}(r)-\rho^N(r)\right)}{\delta}, \quad (3)$$

where *N* stands for the number of electrons in reference state of the molecule, while δ stands for the fraction of electron which default value is set to be 0.01 [90]. Color coding describes how electron density changes with the addition or removal of charge. Namely, the positive

(purple) color indicates that the electron density increases in the case of Fukui f^+ function, while negative (red) color indicates that electron density decreases in the case of Fukui f^- function. Fukui functions of 8HQ5SA molecule are presented in Fig.7. Purple color in Fig.7a determines near vicinities of three hydrogen atoms as molecule sites where electron density increases after the addition of charge. These hydrogen atoms are H6, H7 and H14 and they could have electrophilic nature during the reactions where 8HQ5SA molecule accepts charge. On the other side negative color in Fig.7b indicates that electron density decreases in the near vicinity of OH group connected to sulfur atom, designating this molecule site as nucleophilic during the interactions where 8HQ5SA molecule donates charge.

4.8 Natural bond orbital analysis

The natural bond orbitals (NBO) calculations were performed using NBO 3.1 program [91] as implemented in the Gaussian09 package at the DFT/B3LYP level in order to understand various second-order interactions and the results are tabulated in tables 3 and 4. The strong interaction $n_1C_4 \rightarrow \pi^*(C_5\text{-}N_{15})$ has the highest E(2) value 59.97 kcal/mol and a very strong interaction has been in $n_2O_{16} \rightarrow \pi^*(C_9\text{-}C_{11})$ with an energy of 37.04 kcal/ mol. Table 4 gives the occupancy of electrons and p-character in significant NBO natural atomic hybrid orbitals.Almost100% p-character was observed in π bonding of $C_5\text{-}N_{15}$,$C_9\text{-}C_{11}$ and the lone pairs of n_1C_4, n_2O_{16} and n_3O_{19}.

4.9 Reactive and degradation properties based on autoxidation and hydrolysis

Sensitivity of 8HQ5SA molecule towards the autoxidation mechanism has been investigated by calculations of BDE for hydrogen abstraction, which is of great importance when it comes to the investigation of degradation mechanisms of pharmaceutically important organic molecules [92-95]. Autoxidation is probable in cases when BDE for hydrogen abstraction is in the certain range, from 70 to 85 kcal/mol. This value is proposed according to the works of Wright et al. [96] and Gryn'ova et al. [97]. However, according to Gryn'ova et al. BDE values between 85 and 90 kcal/mol are questionable, but could be of importance to some extent for the autoxidation mechanism. BDE values lower than 70 kcal/mol are not suitable for autoxidation mechanism [96, 98, 99]. Fig.8 contains information about BDE values for hydrogen abstraction and BDE for the rest of the single acyclic bonds. The analysis of BDE for hydrogen abstraction in the case of 8HQ5SA molecule clearly indicates its great stability and very low sensitivity towards autoxidation mechanism. Namely, all BDE values for hydrogen abstraction are much higher than the upper border value of 90 kcal/mol, meaning that the title molecule is highly stable in

the open air and in the presence of oxygen. However, this also means that degradation via autoxidation mechanism is hard to be expected, further meaning that advanced oxidation processes might be necessary for its removal from water. On the other side the lowest BDE values for the rest of the single acyclic bonds have been calculated in the case of bonds denoted with numbers 8 and 10. This indicates that the degradation could start by detaching of OH group connected to the sulfur atom or by detaching of the whole moiety containing sulfur atom. The presence of two OH groups indicates that 8HQ5SA molecule could have pronounced interactions with water molecules, as indicated by the ALIE surface. In this regard we decided to investigate its interactions with water by calculations of radial distribution functions (RDF). RDF, g(*r*), indicates the probability of finding a particle in the distance *r* from another particle [100], and for 8HQ5SA molecule it has been established that total of eight atoms have pronounced interactions with water molecules, Fig.S2 (supporting information). Results presented in Fig.S2 indicate that three carbon atoms, C1, C5 and C11, and sulfur atom, S18, have relatively pronounced interactions with water molecules characterized with similar g(*r*) profiles. Namely, three aforementioned carbon atoms have maximal g(*r*) values between 1.1 and 1.2, while their peak distances are located at around 3.5 Å. Sulfur atom has maximal g(r) value of around 1.2, while its peak distance is located at around 4 Å. As expected, non-carbon atoms of 8HQ5SA molecule have much more pronounced interactions with water molecules. Oxygen atoms O16 and O21 have very similar g(*r*) profiles, with O16 having somewhat higher maximal g(*r*) value (almost 1.3), while O21 has somewhat shorter peak distance (~2.5 Å). H17 is characterized by two distinct solvation spheres with peak distances at around 2.0 and 3.3 Å. By all means the most important atom, from the aspect of interactions with water molecules, is hydrogen atom H22, which is characterized by maximal g(r) value of 2.4 and peak distance located at around 1.5 Å.

4.10 Molecular Docking

The PASS (Prediction of Activity Spectra) [101] analysis of 8HQ5SA is given in the table 5 with appropriate probability values i.e. probable activity (Pa) and probable inactivity (Pi). The present investigation is limited to Monodehydroascorbate reductase (NADH) inhibitor which gave Pa (probability of activity) value of 0.974 for the docking study. The three dimensional structure of Monodehydroascorbate reductase (NADH) inhibitor were retrieved from the protein databank (PDB) with PDB ID 5CP8. NADH-FR system is important for maintaining mitochondrial energy production in tumor microenvironments and used as a novel therapeutic target in tumor [102]. Several literature survey exhibit the anti-

cancerous activity of quinoline derivatives [103,104] and the 8HQ5SA as ligand was prepared for docking by minimizing its energy at B3LYP/6-31G (6D, 7F) level of theory. Molecular docking calculations were carried out using Auto dock Vina software [105]. A molecular format conversion program, Open BabelGUI, was used to prepare ligands for docking processes. Both ligand and receptor were respectively loaded into Auto Dock Tools 1.5.6 software for pre-docking processing, such as water molecules, hetero atoms were removed from the structures, add polar hydrogen's, calculate Gasteiger charges [106], specify rotatable bond for ligand, and so on. The active site of the enzyme was defined to include residues of the active site within the grid size of 40 × 40 × 40 points with 0.375Å spacing on each axis. The optimal binding conformation was determined by LGA (Lamarckian Genetic Algorithm). Finally, the binding mode analysis performed in Discovery Studio Visualizer 4.0 software. The ligand binds at the active site of the substrate by weak non-covalent interactions and these interactions are depicted in Fig.S3 (supporting information). Amino acid Met98 form one H-bond with OH group attached to the quinoline ring. Three pi-alkyl interactions between the phenyl ring and three amino acids Leu197, Ala198 and Ala201.Carbonyl group in Leu197 and Nitrogen in Ala198 form an amide-pi stacked (hydrophobic) interaction with phenyl ring. Ala198 form a pi-alkyl interaction with the quinoline ring. The docked ligand forms a stable complex with NADH inhibitor (Fig. 9) and got a binding affinity value of -6.0 kcal/mol (Table 6). Thus 8HQ5SA can be a lead compound for developing new anti-cancerous drug.

5. Conclusion

The vibrational spectroscopic analysis (FT-IR, FT-Raman and SERS) of 8-hydroxyquinoline-5-sulphonic acid are reported. The sulpho and hydroxyl modes in the SERS spectrum suggest that the interaction between PhI is more than the interaction of PhII with the metal. The sulfonyl group is tilted from the phenyl ring. Using NBO analysis the stability of 8HQ5SA arising from hyperconjugative interactions and charge delocalization have been analyzed. From the MEP plot, the regions of negative potential are over the electro negative oxygen atoms and the regions having the positive potential are over the hydrogen atoms of the OH groups. ALIE values mapped to the electron density surface indicate near vicinities of atoms N15 and C12 as the most sensitive towards the electrophilic attacks. On the other side Fukui functions also recognize atoms H6, H7 and H14 together with OH group as important reactive centers. BDE values for hydrogen abstraction indicate that 8HQ5SA molecule is not sensitive towards autoxidation mechanism, while BDE values for the rest of the single acyclic are the lowest in the case of bond connecting the OH group with sulfur

atom, indicating that degradation could start by detaching of aforementioned OH group. This is very important result since hydrogen atom H22, belonging to the aforementioned OH group, has very pronounced interactions with water molecules which suggests that hydrolysis could have important role in the degradation of title molecule. Carbonyl group in Leu197 and nitrogen in Ala198 form an amide-pi stacked (hydrophobic) interaction with phenyl ring and the Ala198 form a pi-alkyl interaction with the quinoline ring.

Acknowledgment

Part of this work has been performed thanks to the support received from Schrödinger Inc. Part of this study was conducted within the projects supported by the Ministry of Education, Science and Technological Development of Serbia, grant numbers OI 171039 and TR 34019

References

[1] C.W. Tang, S.A. Van Slyke, Organic electroluminescent diodes, Appl. Phys. Lett. 51 (1987) 913-915.

[2] G. Bandoli, A. Dolmella, F. Tisato, M. Porchia, F. Refosco, Mononuclear six coordinated Ga(III) complexes, a comprehensive survey, Coord. Chem. Rev. 253 (2009) 56-77.

[3] L.E. Scott, C. Orvig, Medicinal inorganic chemistry approaches to passivation and removal of aberrant metal ions in disease, Chem. Rev. 109 (2009) 4885-4910.

[4] M.J. Hannon, Metal based anticancer drugs, from a past anchored in platinum chemistry to a post genomic future of diverse chemistry and biology, Pure Appl. Chem. 79 (2007) 2243-2261.

[5] W.E. Ohnesorge, L.B. Rogers, Fluorescence of some metal chelate compounds of 8-quinolinol-I: Effect of metallic ion and solvent on spectrum and quantum yield, Spectrochim. Acta 15 (1959) 27-40.

[6] J.A. Bishop, The use of fluorescence in determining formation constants of complexes: Part II. Complexes which fluoresce, Anal. Chim. Acta 63 (1973) 305-311.

[7] F.E. Lytle, D.R. Storey, M.E. Juricich, Systematic atomic number effects in complexes exhibiting ligang luminescence, Spectrochim. Acta 29 (1973) 1357-1369.

[8] K. Hiraki, K. Morischige, Y. Nishikawa, Simultaneous determinations of metal 5-sulfo-8-quinolinolates by differences in their fluorescence lifetimes, Anal. Chim. Acta 97 (1978) 121-128.

[9] L. Vitali, I.C. Vieira, A. Spinelli, Sensor-containing microspheres of chitosan crosslinked with 8-hydroxyquinoline-5-sulphonic acid for determination of Cu(II) in instant coffee, Food Chem. 126 (2011) 807-814.

[10] R.T. Ulahannan, C.Y. Panicker, H.T. Varghese, R. Musiol, J. Jampilek, C. Van Alsenoy, J.A. War, S.K. Srivastava, Molecular structure, FT-IR, FT-Raman, NBO, HOMO and LUMO, MEP, NLO and molecular docking study of 2-[(E)-2-(2-bromophenyl)-ethenyl]quinoline-6-carboxylic acid, Spectrochim. Acta 151 (2015) 184-197.

[11] R.T. Ulahannan, C.Y. Panicker, H.T. Varghese, R. Musiol, J. Jampilek, C. Van Alsenoy, J.A. War, T.K. Manojkumar, Vibrational spectroscopic studies and molecular docking study of 2-[(E)-2-phenylethenyl]quinoline-5-carboxylic acid, Spectrochim. Acta 151 (2015) 190-199.

[12] R.T. Ulahannan, C.Y. Panicker, H.T. Varghese, R. Musiol, J. Jampilek, C. Van Alsenoy, J.A. War, A.A. Al-Saadi, Vibrational spectroscopic and molecular docking study of (2E)-N-(4-chloro-2-oxo-1,2-dihydroquinolin-3-yl)-3-phenylprop-2-enamide, Spectrochim. Acta 151 (2015) 335-349.

[13] E. Fazal, C.Y. Panicker, H.T. Varghese, S. Nagarajan, B.S. Sudha, J.A. War, S.K. Srivastava, B. Harikumar, P.L. Anto, Spectroscopic investigation (FT-IR, FT-Raman), HOMO-LUMO, NBO analysis and molecular docking study of 4-chlorophenyl quinoline-2-carboxylate, Spectrochim. Acta 145 (2015) 260-269.

[14] E. Fazal, C.Y. Panicker, H.T. Varghese, S. Nagarajan, B.S. Sudha, J.A. War, S.K. Srivastava, B. Harikumar, P.L. Anto, Vibrational spectroscopic and molecular docking study of 4-methylphenylquinoline-2-carboxylate, Spectrochim. Acta 143 (2015) 213-222.

[15] R.T. Ulahannan, C.Y. Panicker, H.T. Varghese, C. Van Alsenoy, R. Musiol, J. Jampilek, P.L. Anto, Vibrational spectroscopic, 1H NMR and quantum chemical computational study of 4-hydroxy-2-oxo-1,2-dihydroquinoline-8-carboxylic acid, Spectrochim. Acta 121 (2014) 445-456.

[16] R.T. Ulahannan, C.Y. Panicker, H.T. Varghese, C. Van Alsenoy, R. Musiol, J. Jampilek, P.L. Anto, Spectroscopic (FT-IR, FT-Raman) investigations and quantum chemical calculations of 4-hydroxy-2-oxo-1,2-dihydroquinoline-7-carboxylic acid, Spectrochim. Acta 121 (2014) 404-414.

[17] S. Armaković, S.J. Armaković, J.P. Šetrajčić, I.J. Šetrajčić, Active components of frequently used β-blockers from the aspect of computational study, J. Mol. Model. 18(9) (2012) 4491-4501.

[18] S.J. Armaković, S. Armaković, N.L. Finčur, F. Šibul, D. Vione, J.P. Šetrajčić, B. Abramović, Influence of electron acceptors on the kinetics of metoprolol

photocatalytic degradation in TiO 2 suspension. A combined experimental and theoretical study, RSC Advances 5(67) (2015) 54589-54604.

[19] M. Blessy, R.D. Patel, P.N. Prajapati, Y. Agrawal, Development of forced degradation and stability indicating studies of drugs-A review., J Pharm. Anal. 4(3) (2014) 159-165.

[20] B. Abramović, S. Kler, D. Šojić, M. Laušević, T. Radović, D. Vione, Photocatalytic degradation of metoprolol tartrate in suspensions of two TiO 2-based photocatalysts with different surface area. Identification of intermediates and proposal of degradation pathways, J. Hazard. Mater. 198 (2011) 123-132.

[21] J. Molnar, J. Agbaba, B. Dalmacija, M. Klašnja, M. Watson, M. Kragulj, Effects of ozonation and catalytic ozonation on the removal of natural organic matter from groundwater, J. Environment. Engineer. 138(7) (2011) 804-808.

[22] J.J. Molnar, J.R. Agbaba, B.D. Dalmacija, M.T. Klašnja, M.B. Dalmacija, M.M. Kragulj, A comparative study of the effects of ozonation and TiO 2-catalyzed ozonation on the selected chlorine disinfection by-product precursor content and structure, Sci. Total Environment, 425 (2012) 169-175.

[23] D.V. Šojić, D.Z. Orčić, D.D. Četojević-Simin, N.D. Banić, B.F. Abramović, Efficient removal of sulcotrione and its formulated compound Tangenta® in aqueous TiO 2 suspension: Stability, photoproducts assessment and toxicity, Chemosphere, 138 (2015) 988-994.

[24] D.V. Šojić, D.Z. Orčić, D.D. Četojević-Simin, V.N. Despotović, B.F. Abramović, Kinetics and the mechanism of the photocatalytic degradation of mesotrione in aqueous suspension and toxicity of its degradation mixtures, J. Mol. Catalysis A: Chem. 392 (2014) 67-75.

[25] D.D. Četojević-Simin, S.J. Armaković, D.V. Šojić, B.F. Abramović, Toxicity assessment of metoprolol and its photodegradation mixtures obtained by using different type of TiO 2 catalysts in the mammalian cell lines, Sci. Total Environ. 463 (2013) 968-974.

[26] P. Lienard, J. Gavartin, G. Boccardi, M. Meunier, Predicting drug substances autoxidation, Pharm. Res. 32(1) (2015) 300-310.

[27] G.L. de Souza, L.M. de Oliveira, R.G. Vicari, A. Brown, A DFT investigation on the structural and antioxidant properties of new isolated interglycosidic O-(1→ 3) linkage flavonols, J. Mol. Model. 22(4) (2016) 1-9.

[28] Z. Sroka, B. Żbikowska, J. Hładyszowski, The antiradical activity of some selected

flavones and flavonols. Experimental and quantum mechanical study, J. Mol. Model. 21(12) (2015) 1-11.

[29] H. Djeradi, A. Rahmouni, A. Cheriti, Antioxidant activity of flavonoids: a QSAR modeling using Fukui indices descriptors, J. Mol. Model. 20(10) (2014) 1-9.

[30] N. Lepold, B. Lendl, A new method for fast preparation of highly surface enhanced Raman scattering (SERS) active silver colloids at room temperature by reduction of silver nitrate with hydroxylamine hydrochloride, J. Phys. Chem. B107 (2003) 5723-5727.

[31] C.P. Lloyd, W.F. Pickering, The reduction of silver salts by hydroxylamine, J. Inorg. Chem. 29 (1967) 1907-1914.

[32] K. Haruna, T.A. Saleh, J.A. Thagfi, A.A. Al-Saadi, Structural properties, vibrational spectra and surface enhanced Raman scattering of 2,4,6-trichloro- and tribromoanilines, a comparative study, J. Mol. Struct. 1121 (2016) 7-15.

[33] Gaussian 09, Revision B.01, M.J. Frisch, G.W. Trucks, H.B. Schlegel, G.E. Scuseria, M.A. Robb, J.R. Cheeseman, G. Scalmani, V. Barone, B. Mennucci, G.A. Petersson, H. Nakatsuji, M. Caricato, X. Li, H.P. Hratchian, A.F. Izmaylov, J. Bloino, G. Zheng, J.L. Sonnenberg, M. Hada, M. Ehara, K. Toyota, R. Fukuda, J. Hasegawa, M. Ishida, T. Nakajima, Y. Honda, O. Kitao, H. Nakai, T. Vreven, J.A. Montgomery, Jr., J.E. Peralta, F. Ogliaro, M. Bearpark, J.J. Heyd, E. Brothers, K.N. Kudin, V.N. Staroverov, T. Keith, R. Kobayashi, J. Normand, K. Raghavachari, A. Rendell, J.C. Burant, S.S. Iyengar, J. Tomasi, M. Cossi, N. Rega, J.M. Millam, M. Klene, J.E. Knox, J.B. Cross, V. Bakken, C. Adamo, J. Jaramillo, R. Gomperts, R.E. Stratmann, O. Yazyev, A.J. Austin, R. Cammi, C. Pomelli, J.W. Ochterski, R L. Martin, K. Morokuma, V.G. Zakrzewski, G A. Voth, P. Salvador, J.J. Dannenberg, S. Dapprich, A.D. Daniels, O. Farkas, J.B. Foresman, J.V. Ortiz, J. Cioslowski, D.J. Fox, Gaussian, Inc., Wallingford CT, 2010.

[34] J.B. Foresman, in: E. Frisch (Ed.), Exploring Chemistry with Electronic Structure Methods: a Guide to Using Gaussian, 1996, Pittsburg, PA.

[35] R. Dennington, T. Keith, J. Millam, GaussView, Version 5, Semichem Inc., Shawnee Mission KS, 2009.

[36] J.M.L. Martin, C. Van Alsenoy, GAR2PED, a Program to Obtain a Potential Energy Distribution from a Gaussian Archive Record, University of Antwerp, Belgium, 2007.

[37] A.D. Bochevarov, E. Harder, T.F. Hughes, J.R. Greenwood, D.A. Braden, D.M. Philipp, D. Rinaldo, M.D. Halls, J. Zhang, R.A. Friesner, Jaguar: A

high-performance quantum software program with strengths in life and materials sciences, Int. J. Quantum Chem., 113(8) (2013) 2110-2142.

[38] A.D. Becke, Density-functional thermochemistry. III. The role of exact exchange, J. Chem. Phys., 98(7) (1993) 5648-5652.

[39] D. Shivakumar, J. Williams, Y. Wu, W. Damm, J. Shelley, W. Sherman, Prediction of absolute solvation free energies using molecular dynamics free energy perturbation and the OPLS force field, J. Chem. Theor. Comput., 6(5) (2010) 1509-1519.

[40] Z. Guo, U. Mohanty, J. Noehre, T.K. Sawyer, W. Sherman, G. Krilov, Probing the α-Helical Structural Stability of Stapled p53 Peptides: Molecular Dynamics Simulations and Analysis, Chem. Biol. Drug Design, 75(4) (2010) 348-359.

[41] K.J. Bowers, E. Chow, H. Xu, R.O. Dror, M.P. Eastwood, B.A. Gregersen, J.L. Klepeis, I. Kolossvary, M.A. Moraes, F.D. Sacerdoti, Scalable algorithms for molecular dynamics simulations on commodity clusters, in SC 2006 Conference, Proceedings of the ACM/IEEE. 2006. IEEE.

[42] I. Fabijanić, C.J. Brala, V. Pilepić, The DFT local reactivity descriptors of α-tocopherol, J. Mol. Model., 21(4) (2015) 1-7.

[43] J.L. Banks, H.S. Beard, Y. Cao, A.E. Cho, W. Damm, R. Farid, A.K. Felts, T.A. Halgren, D.T. Mainz, J.R. Maple, Integrated modeling program, applied chemical theory (IMPACT), J. Comput. Chem., 26(16) (2005) 1752-1780.

[44] H.J. Berendsen, J.P. Postma, W.F. van Gunsteren, J. Hermans, Interaction models for water in relation to protein hydration, in Intermolecular forces, 1981, Springer. p. 331-342.

[45] A. Otero-de-la-Roza, E.R. Johnson, J. Contreras-García, Revealing non-covalent interactions in solids: NCI plots revisited, Phys. Chem. Chem. Phys., 14(35) (2012) 12165-12172.

[46] E.R. Johnson, S. Keinan, P. Mori-Sanchez, J. Contreras-Garcia, A.J. Cohen, W. Yang, Revealing noncovalent interactions, J. Am. Chem. Soc., 132(18) (2010) 6498-6506.

[47] Schrödinger Release 2015-4: Maestro, version 10.4, Schrödinger, LLC, New York, NY, 2015.

[48] L.L. Merritt, B. Duffin, The crystal structures of two derivatives of 8-

hydroxyquinoline-5-sulfonic acid, 2-methyl-8-hydroxyquinoline-5-sulfonic acid monohydrate and 7-iodo-8-hydroxyquinoline-5-sulfonic acid, Acta Cryst. B26 (1970) 734-744.

[49] P.T. Muthiah, S. Murugesan, Synthesis and crystal structures of lithium 8-hydroxyquinoline-5-sulfonate tetrahydrate, J. Coord. Chem. 59 (2006) 1167-1172.

[50] G. Smith, U.D. Wermuth, P.C. Healy, Proton transfer compounds of 8-hydroxy-7-iodoquinoline-5-sulfonic acid (ferron) with 4-chloroaniline and 4-bromoaniline, Acta Cryst. C63 (2007) o405-407.

[51] N.P.G. Roeges, A Guide to the Complete Interpretation of Infrared Spectra of Organic Structures, John Wiley and Sons., New York, 1994.

[52] N.B. Colthup, L.H. Daly, S.E. Wiberly, Introduction to Infrared and Raman Spectroscopy, Academic Press, New York, 1990.

[53] G. Varsanyi, Assignments for Vibrational Spectra of Seven Hundred Benzene Derivatives, Wiley, New York, 1974.

[54] R. Renjith, Y.S. Mary, H.T. Varghese, C.Y. Panicker, T. Thiemann, A. Shereef, A.A. Al-Saadi, Spectroscopic investigation (FT-IR an dFT-Raman), vibrational assignments, HOMO-LUMO analysis and molecular docking study of 1-hydroxy-4,5,8-tris(4-methoxyphenyl)anthraquinone, J. Phys. Chem. Solids 87 (2015) 110-121.

[55] S. Muthu, J. Uma Maheswari, T. Sundius, Quantum mechanical, spectroscopic studies (FT-IR, FT-Raman, NMR, UV) and normal coordinate analysis of 3-([2-(diaminomethylenemino)thiazol-4-yl)methylthio)-N-sulfamoylpropanimidamide, Spectrochim. Acta 108 (2013) 307-318.

[56] S. Sebastian, S. Sylvestre, N. Sundaraganesan, M. Amalanathan, S. Ayyapan, K. Oudayakumar, B. Karthikeyan, Vibrational spectra, molecular structure, natural bond orbital, first order hyperpolarizability, TD-DFT and thermodynamic analysis of 4-amino-3-hydroxy-1-naphthalenesulfonic acid by DFT approach, Spectrochim. Acta 107 (2013) 167-178.

[57] A. Chandran, Y.S. Mary, H.T. Varghese, C.Y. Panicker, P. Pazdera, G. Rajendran, FT-IR, FT-Raman spectroscopy and computational study of (E)-4-((anthracen-9-ylmethylene)amino)-N-carbamimidoylbenzene sulfonamide, Spectrochim. Acta 79 (2011) 1584-1592.

[58] S.M. Chackalackal, F.E. Stafford, Infrared spectra of methane-, fluoro-, and chlorosulfonic acids, J. Am. Chem. Soc. 88 (1966) 4815-4819.

[59] C.Y. Panicker, H.T. Varghese, D. Philip, H.I.S. Nogueira, FT-IR, FT-Raman and SERS spectra of pyridine-3-sulfonic acid, Spectrochim. Acta 64 (2006) 744-747.

[60] A. Chandran, Y.S. Mary, H.T. Varghese, C.Y. Panicker, P. Pazdera, G. Rajendran, N. Babu, FT-IR, FT-Raman spectroscopy and computational study of N-carbamimidoyl-4-{[(E)-((2-hydroxyphenyl) methylidene] amino} benzene sulfonamide, J. Mol. Struct. 992 (2011) 77-83.

[61] Y.S. Mary, C.Y. Panicker, P.L. Anto, M. Sapnakumari, B. Narayana, B.K. Sarojini, Molecular structure, FT-IR, NBO, HOMO and LUMO, MEP and first order hyperpolarizability of (2E)-1-(2,4-dichlorophenyl)-3-(3,4,5-trimethoxyphenyl)prop-2-en-1-one by HF and density functional methods, Spectrochim. Acta 135 (2015) 81-92.

[62] C.Y. Panicker, H.T. Varghese, D. Philip, H.I.S. Nogueira, K. Castkova, Raman, IR and SERS spectra of methyl(2-methyl-4,6-dinitrophenylsulfanyl)ethanoate, Spectrochim. Acta 67 (2007) 1313-1320.

[63] G. Socrates, Infrared and Raman Characteristic Group Frequencies, Wiley, Middlesex, UK, 2001.

[64] J. Gao, H. Gu, B. Xu, Multifunctional magnetic nanoparticles, design, synthesis and biomedical applications, Acc. Chem. Res. 42 (2009) 1097-1107.

[65] C.K. Kim, P. Ghosh, C. Pagliuca, Z. Zhu, S. Menichetti, V.M. Rotello, Entrapment of hydrophobic drugs in nanoparticle monolayers with efficient release into cancer cells, J. Am. Chem. Soc. 131 (2009) 1360-1361.

[66] S. Zong, Z. Wang, H. Chen, J. Yang, Y. Cui, Surface enhanced Raman scattering traceable and glutathione responsive nanocarrier for the intracellular drug discovery, Anal. Chem. 85 (2013) 2223-2230.

[67] H.T. Varghese, C.Y. Panicker, D. Philip, J.R. Mannekutla, S.R. Inamdar, IR, Raman and SERS studies of methyl salicylate, Spectrochim. Acta 66 (2007) 959-963.

[68] Y. Fleger, Y. Mastai, M. Rosenbluh, D.H. Dressler, Surface enhanced Raman spectroscopy of aromatic compounds on silver nanoclusters, Surf. Sci. 603 (2009) 788-793.

[69] Y.S. Mary, P.J. Jojo, C. Van Alsenoy, M. Kaur, M.S. Siddegowda, H.S. Yathirajan, H.I.S. Nogueira, S.M.A. Cruz, Vibrational spectroscopic studies (FT-IR, FT-Raman, SERS) and quantum chemical calculations on cyclobenzaprinium salicylate, Spectrochim. Acta 120 (2014) 340-350.

[70] Y.S. Mary, P.J. Jojo, C. Van Alsenoy, M. Kaur, M.S. Siddegowda, H.S. Yathirajan,

H.I.S. Nogueira, S.M.A. Cruz, Vibrational spectroscopic (FT-IR, FT-Raman, SERS) and quantum chemical calculations of 3-(10,10-dimethyl-anthracen-9-ylidene)-N,N,N-trimethylpropanaminiium chloride (Melitracenium chloride), Spectrochim. Acta 120 (2014) 370-380.

[71] M. Moskovits, Surface enhanced spectroscopy, Rev. Mod. Phys. 57 (1985) 783-825.

[72] M. Moskovits, D.P. DiLella, K.J. Maynard, Surface Raman spectroscopy of a number of cyclic aromatic molecules adsorbed on silver, selection rules and molecular reorientation, Langmuir, 4 (1988) 67-76.

[73] J. Munoz-Perez, P. Leyton, C. Paipa, J.P. Soto, J. Brunet, J.S. Gomez-Jeria, M.M. Campos-Vallette, Raman and surfaced Raman scattering study of the orientation of cruciform 9,10-anthracene thiophene and furan derivatives deposited on a gold colloidal surface, J. Mol. Struct. 1122 (2016) 198-204.

[74] C.Y. Panicker, H.T. Varghese, L. Ushakumary, IR, Raman and SERS spectra of ethyl salicylate, J. Raman Spectrosc. 40 (2009) 2023-2030.

[75] P.L. Anto, R.J. Anto, H.T. Varghese, C.Y. Panicker, D. Philip, A.G. Brolo, FT-IR, FT-Raman and SERS spectra of anilinum sulfate, J. Raman Spectrosc. 40 (2009) 1810-1815.

[76] C. Garrido, G. Diaz-Fleming, M.M. Campos-Vallette, SERS spectrum of gallic acid obtained from a modified silver colloid, Spectrochim. Acta 163 (2016) 68-72.

[77] Y.S. Mary, H.T. Varghese, C.Y. Panicker, M. Girisha, B.K. Sagar, H.S. Yathirajan, A.A. Al-Saadi, C. Van Alsenoy, Vibrational spectra, HOMO, LUMO, NBO, MEP analysis and molecular docking study of 2,2-diphenyl-4-(piperidin-1-yl)butanamide, Spectrochim. Acta A 150 (2015) 543-556.

[78] C. Adant, M. Dupuis, J.L. Bredas, Ab initio study of the nonlinear optical properties of urea, electron correlation and dispersion effects, Int. J. Quantum Chem. 56 (1995) 497-507.

[79] A. Chandran, H.T. Varghese, C.Y. Panicker, T.K. Manojkumar, C. Van Alsenoy, G. Rajendran, FT-IR, FT-Raman and quantum chemical calculations of (E)-N-carbamimidoyl-4-((3,4-dimethoxybenzylidene)amino)benzenesulfonamide, Spectrochim. Acta 84 (2011) 156-163.

[80] K. Fukui, Theory of Orientation and Stereoselections, Springer-Verlag, New York, 1975.

[81] J.A. War, K. Jalaja, Y.S. Mary, C.Y. Panicker, S. Armakovic, S.J. Armakovic, S.K. Srivastava, C. Van Alsenoy, Spectroscopic characterization of 1-[3-(1*H*-imidazol-1-

yl)propyl]-3-phenylthiourea and assessment of reactive and optoelectronic properties employing DFT calculations and molecular dynamics simulations, J. Mol. Struct. 1129 (2017) 72-85.

[82] A.H. Pandith, N. Islam (2014) Electron Transport and Nonlinear Optical Properties of Substituted Aryldimesityl Boranes: A DFT Study. PLoS ONE 9(12) : e114125. doi:10.1371/ journal.pone.0114125.

[83] R.G. Parr, R,G. Pearson, Absolute hardness: companion parameter to absolute electronegativity , J. Am. Chem. Soc. 105 (1983) 7512-7516.

[84] R.P. Verma, C. Hansch, A comparison between two polarizability parameters in chemical biological interactions, Bioorg. Med. Chem. 13 (2005) 2355-2372.

[85] K. Srivastava, A. Srivastava, P. Tandon, K. Sinha, J. Wang, Spectroscopic, quantum chemical calculation and molecular docking of dipfluzine, J. Mol. Struct. 1125 (2016) 751-762.

[86] J.S. Murray, J.M. Seminario, P. Politzer, P. Sjoberg, Average local ionization energies computed on the surfaces of some strained molecules, Int. J. Quantum Chem. 38(S24) (1990) 645-653.

[87] P. Politzer, F. Abu-Awwad, J.S. Murray, Comparison of density functional and Hartree–Fock average local ionization energies on molecular surfaces, Int. J. Quantum Chem. 69(4) (1998) 607-613.

[88] F.A. Bulat, A. Toro-Labbé, T. Brinck, J.S. Murray, P. Politzer, Quantitative analysis of molecular surfaces: areas, volumes, electrostatic potentials and average local ionization energies, J. Mol. Model. 16(11) (2010) 1679-1691.

[89] P. Politzer, J.S. Murray, F.A. Bulat, Average local ionization energy: a review, J. Mol. Model. 16(11) (2010) 1731-1742.

[90] A. Michalak, F. De Proft, P. Geerlings, R. Nalewajski, Fukui functions from the relaxed Kohn-Sham orbitals, J. Phys. Chem. A, 103(6) (1999) 762-771.

[91] E.D. Glendening, A.E. Reed, J.E. Carpenter, F. Weinhold, NBO Version 3.1, Gaussian Inc., Pittsburgh, PA, 2003.

[92] X. Ren, Y. Sun, X. Fu, L. Zhu, Z. Cui, DFT comparison of the OH-initiated degradation mechanisms for five chlorophenoxy herbicides, J. Mol. Model. 19(6) (2013) 2249-2263.

[93] L.-l. Ai, J.-y. Liu, Mechanism of OH-initiated atmospheric oxidation of E/Z-CF3CF= CFCF3: a quantum mechanical study, J. Mol. Model. 20(4) (2014) 1-10.

[94] W. Sang-aroon, V. Amornkitbamrung, V. Ruangpornvisuti, A density functional theory study on peptide bond cleavage at aspartic residues: direct vs cyclic intermediate hydrolysis, J. Mol. Model. 19(12) (2013) 5501-5513.

[95] J. Kieffer, E. Brémond, P. Lienard, G. Boccardi, In silico assessment of drug substances chemical stability, J. Mol. Struct. THEOCHEM. 954(1) (2010) 75-79.

[96] J.S. Wright, H. Shadnia, L.L. Chepelev, Stability of carbon-centered radicals: Effect of functional groups on the energetics of addition of molecular oxygen, J. Comput. Chem. 30(7) (2009) 1016-1026.

[97] G. Gryn'ova, J.L. Hodgson, M.L. Coote, Revising the mechanism of polymer autoxidation, Org. Biomol. Chem. 9(2) (2011) 480-490.

[98] P. Lienard, J. Gavartin, G. Boccardi, M. Meunier, Predicting drug substances autoxidation, Pharm. Res. 32(1) (2015) 300-310.

[99] T. Andersson, A. Broo, E. Evertsson, Prediction of Drug Candidates' Sensitivity Toward Autoxidation: Computational Estimation of C-H Dissociation Energies of Carbon-Centered Radicals, J. Pharm. Sci. 103(7) (2014) 1949-1955.

[100] R.V. Vaz, J.R. Gomes, C.M. Silva, Molecular dynamics simulation of diffusion coefficients and structural properties of ketones in supercritical CO 2 at infinite dilution, J. Supercritic. Fluids, 107 (2016) 630-638.

[101] A. Lagunin, A. Stepanchikova, D. Filimonov, V. Poroikov, PASS: prediction of activity spectra for biologically active substances, Bioinformatics, 16(8) (2000) 747-748.

[102] E. Tomitsuka, K. Kita, H. Esumi, An anticancer agent, pyrvinium pamoate inhibits the NADH-fumarate reductase system--a uniquemitochondrial energy metabolism in tumour microenvironments, J. Biochem. 152(2) (2012) 171-183.

[103] M. Ghorab, F.A. Ragab, H.I. Heiba, W.M. Ghorab, Design and synthesis of some novel quinoline derivatives as anticancer and radio sensitizing agents targeting VEGFR tyrosine kinase, J. Heterocy. Chem. 48 (2011) 1269-1279.

[104] M. Bingul, O. Tan, C.R. Gardner, S.K. Sutton, G.M. Arndt, G.M. Marshall , B.B. Cheung , N. Kumar, D.S. Black , Synthesis, Characterization and Anti-Cancer Activity of Hydrazide Derivatives Incorporating a Quinoline Moiety, Molecules 21 (2016) 916.

[105] O. Trott, A. J. Olson, AutoDock Vina: Improving the speed and accuracy of docking

with a new scoring function, efficient optimization and multithreading, J. Comput. Chem. 31 (2010) 455-461.

[106] J.Gasteiger, M.Marsili, Iterative partial equalization of orbital electronegativity - a rapid access to atomic charges, Tetrahedron 36 (1980) 3219-3228.

Figure captions

Fig.1 FT-IR spectrum of 8HQ5SA

Fig.2 FT-Raman spectrum of 8HQ5SA

Fig.3 SERS spectrum of 8HQ5SA

Fig.4 Optimized geometry of 8HQ5SA

Fig.5 HOMO-LUMO plots of 8HQ5SA

Fig.6 ALIE surface of 8HQ5SA molecule

Fig.7 Fukui functions a) f^{+} and b) f^{-} of the 8HQ5SA molecule

Fig.8 BDEs of all single acyclic bonds of 8HQ5SA molecule

Fig.9 Surface view of the docked ligand embedded in the catalytic site of NADH inhibitor

Table1

Geometrical parameters (DFT) of 8-hydroxyquinoline-5-sulphonic acid

Bond lengths (Å)

C1-C2	1.3793	C1-C5	1.4155	C1-H6	1.0894
C2-C3	1.4213	C2-H7	1.0869	C3-C4	1.4260
C3-C8	1.4300	C4-C9	1.4360	C4-N15	1.3586
C5-H10	1.0919	C5-N15	1.3202	C8-C12	1.3838
C8-S18	1.7873	C9-C11	1.3831	C9-O16	1.343
C11-C12	1.4092	C11-H13	1.0882	C12-H14	1.0883
O16-H17	0.9788	S18-O19	1.4846	S18-O20	1.4786
S18-O21	1.6775	O21-H22	0.9729		

Bond angles (°)

C2-C1-C5	119.7	C2-C1-H6	120.7	C5-C1-H6	119.6
C1-C2-C3	119.2	C1-C2-H7	120.8	C3-C2-H7	120.0
C2-C3-C4	116.3	C2-C3-C8	126.6	C4-C3-C8	117.0
C3-C4-C9	120.6	C3-C4-N15	123.8	C9-C4-N15	115.6
C1-C5-H10	120.3	C1-C5-N15	122.8	H10-C5-N15	116.8
C3-C8-C12	121.4	C3-C8-S18	121.9	C12-C8-S18	116.7
C4-C9-C11	120.3	C4-C9-O16	118.3	C11-C9-O16	121.4
C9-C11-C12	119.4	C9-C11-H13	119.9	C12-C11-H13	120.7
C8-C12-C11	121.2	C8-C12-H14	119.0	C11-C12-H14	119.8 \
C4-N15-C5	118.1	C9-O16-H17	105.9	C8-S18-O19	112.1
C8-S18-O20	109.7	C8-S18-O21	98.1	O19-S18-O20	119.5
O19-S18-O21	106.6	O20-S18-O21	108.5	S18-O21-H22	106.8

Dihedral angles (°)

C5-C1-C2-C3	-0.1	C5-C1-C2-H7	178.9	H6-C1-C2-C3	-179.9
H6-C1-C2-H7	-0.9	C2-C1-C5-H10	-180.0	C2-C1-C5-N15	-0.1
H6-C1-C5-H10	-0.2	H6-C1-C5-N15	179.7	C1-C2-C3-C4	0.2
C1-C2-C3-C8	-179.7	H7-C2-C3-C4	-178.8	H7-C2-C3-C8	1.3
C2-C3-C4-C9	179.7	C2-C3-C4-N15	-0.2	C8-C3-C4-C9	-0.3
C8-C3-C4-N15	179.8	C2-C-3C8-C12	-179.9	C2-C3-C8-S18	-0.1

C4-C3-C8-C12	0.2	C4-C3-C8-S18	179.9	C3-C4-C9-C11	0.1
C3-C4-C9-O16	-179.8	N15-C4-C9-C11	-180.0	N15-C4-C9-O16	0.1
C3-C4-N15-C5	0.0	C9-C4-N15-C5	-179.9	C1-C5-N15-C4	0.1
H10-C5-N15-C4	-180.0	C3-C8-C12-C11	0.2	C3-C8-C12-H14	179.9
S18-C8-C12-C11	-179.5	S18-C8-C12-H14	0.2	C3-C8-S18-O19	-40.2
C3-C8-S18-O20	-175.5	C3-C8-S18-O21	71.4	C12-C8-S18-O19	139.5
C12-C8-S18-O20	4.3	C12-C8-S18-O21	-108.8	C4-C9-C11-C12	0.3
C4-C9-C11-H13	-179.9	O16-C9-C11-C12	-179.8	O16-C9-C11-H13	0.0
C4-C9-O16-H17	-0.0	C11-C9-O16-H17	-180.0	C9-C11-C12-C8	-0.5
C9-C11-C12-H14	179.8	H13-C11-C12-C8	179.7	H13-C11-C12-H14	0.0
C8-S18-O21-H22	-166.7	O19-S18-O21-H22	-50.7	O20-S18-O21-H22	79.2

Table 2

Calculated scaled wavenumbers, observed IR, Raman, SERS bands and assignments of 8-hydroxyquinoline-5-sulphonic acid

B3LYP/aug-cc-pVDZ			IR	Raman	SERS	Assignments[a]
υ(cm^{-1})	IR_I	R_A	υ(cm^{-1})	υ(cm^{-1})	υ(cm^{-1})	-
3587	110.80	218.34	3550	-	-	υOH(100)
3447	120.80	85.32	3440	-	-	υOH(100)
3107	2.93	75.11	3105	3109	3120	υCHII(95)
3097	5.00	144.29	-	-	-	υCHI(99)
3085	1.35	87.40	-	-	3087	υCHI(99)
3078	7.54	185.21	3076	3077	-	υCHII(90)
3044	14.07	149.46	3025	-	-	υCHII(94)
1601	23.93	8.64	1602	1603	1628	υPhI(52), υCCII(22)
1571	11.03	5.35	-	-	1565	υCCII(36), υCNII(16)
1544	36.53	86.12	1550	1547	1528	υCNII(13), υPhI(42), υCCII(16)
1476	255.20	14.76	1482	1472	1481	υPhI(44), υCCII(21)
1436	42.23	9.52	1429	-	1430	υPhI(40), υCNII(10), δCHI(15)
1400	14.11	100.97	-	1408	1395	υPhI(15), δOH(39), δCHII(11)
1368	6.83	8.92	1372	1372	-	δCHII(36), υPhI(14), δCHI(12)
1349	42.27	2.90	-	-	-	δCHII(47), υCNII(20), υPhI(21)
1334	37.95	91.02	-	1324	1328	υPhI(48), υCNII(11), υCCII(18)
1255	114.67	15.16	-	1260	1280	υCO(36), υCNII(38)
1237	3.62	4.00	1233	-	1240	υCNII(42), υPhI(17)
1213	166.25	7.26	-	1217	1212	υSO_2(78)
1187	141.94	11.79	1190	1185	-	δSOH(39), υPhI(16),

						υCNII(10), υCCII(10), δCHII(20)
1172	38.07	6.99	1169	1170	1178	δCHI(39), υPhI(23), υCCII(10), δCHII(10)
1127	20.10	2.59	1130	1130	-	δCHII(44), δCHI(19)
1116	197.80	33.78	-	-	-	υSO_2(10), δCHII(22), υPhI(18)
1098	18.02	1.98	1093	1094	1105	δCHI(40), υPhI(15), δCHII(17)
1052	6.13	7.42	1055	-	1055	υCCII(34), υPhI(11), δCHI(21)
1030	75.87	8.50	1035	1035	-	υSO_2(62)
1017	15.13	23.73	-	-	-	υPhI(42)
970	0.54	0.89	972	977	980	γCHII(85), τPhII(10)
954	0.08	0.30	953	957	-	γCHI(83), δPhI(11)
935	0.47	0.30	-	-	-	γCHII(89)
915	15.70	0.78	-	908	-	δPhII(14), δPhI(16), υCCII(35)
845	14.22	0.47	851	840	835	τPhI(20), γCHI(50), τPhII(14)
820	2.09	0.74	820	818	-	τPhII(15), γCHI(21), τPhI(22), γCHII(11)
793	11.86	1.79	802	-	-	δPhII(45), δPhI(13)
781	49.36	0.30	779	782	-	γCHII(72)
704	46.61	35.53	713	-	740	δPhI(18), υSO(28), δSO_2(10)
699	204.42	6.85	692	702	701	υSO(53), δSO_2(12)
671	79.56	1.39	-	677	-	τOH(84)
641	6.27	0.12	-	647	-	τPhII(38), τPhI(19), γCO(24)
633	21.85	9.01	633	-	-	δPhII(24), δPhI(17),

						υCS(33)
601	1.89	0.35	599	597	605	δPhI(20), γCS(17), τPhII(15), γCO(13)
554	16.16	2.98	555	552	560	δPhII(40), δCO(19), δCS(10)
535	5.96	17.54	537	-	-	δPhII(27), δCS(13), δSO_2(26)
493	116.98	2.71	491	-	510	δSO_2(49), δPhI(27)
476	3.03	5.34	-	-	-	δPhI(56), δPhII(18)
470	2.23	0.46	471	469	-	τPhII(36), τPhI(33), δSO_2(11)
450	10.58	1.66	452	-	-	δSO_2(39), τPhI(26), τPhII(11)
414	4.14	1.45	416	416	420	τPhII(61), γCO(15)
406	18.52	2.99	-	404	-	δSO_2(61)
357	7.37	0.99	-	358	365	δSO_2(46), τPhI(24)
297	4.66	2.95	-	299	309	δCO(33), δSO_2(27), δPhI(11)
267	9.63	5.18	-	267	-	δSO_2(38), δPhI(22)
249	1.58	3.74	-	-	-	δCO(18), δPhI(33), δSO(12)
225	0.29	1.15	-	-	220	δSO_2(36), τPhII(29)
170	3.72	0.31	-	-	177	τPhII(30), γCS(17), τPhI(30)
151	0.18	0.92	-	155	-	τPhI(36), δCS(29)
143	0.10	0.96	-	141	-	τPhI(38), δCS(19), τPhII(26)
88	66.47	1.73	-	-	-	τSO(54), δSO_2(13)
74	3.14	4.01	-	72	-	γCS(35), τPhI(23), τPhII(10)
46	0.23	1.40	-	-	-	τSO_2(76)

[a]υ-stretching; δ-in-plane deformation; γ-out-of-plane deformation; τ-torsion; PhI-C_3-C_4-C_9-C_{11}-C_{12}-C_8; PhII-C_1-C_2-C_3-C_4-N_{15}-C_5; potential energy distribution (%) is given in brackets in the assignment column; IR_I - IR intensity in KM/Mole; R_A-Raman activity in $Å^4$/AMU.

Table 3. Second-order perturbation theory analysis of Fock matrix in NBO basis corresponding to the intramolecular bonds of the title compound

Donor(i)	Type	ED/e	Acceptor(j)	Type	ED/e	E(2)[a]	E(j)-E(i)[b]	F(i,j)[c]
C3-C4	σ	1.96717	C3-C8	σ*	0.03156	3.53	1.22	0.058
-	-	-	C4-C9	σ*	0.04215	2.83	1.20	0.052
-	-	-	C8-S18	σ*	0.19132	3.90	0.86	0.054
C4-C9	σ	1.97627	C3-C4	σ*	0.03973	2.58	1.22	0.050
-	-	-	C5 -N15	σ*	0.01320	3.03	1.26	0.055
-	-	-	C9-C11	σ*	0.02196	2.91	1.27	0.054
C5-C15	σ	1.98775	C4 -C9	σ*	0.04215	2.80	1.35	0.055
-	-	-	C4 -N15	σ*	0.02079	1.70	1.35	0.043
C8-C18	σ	1.96254	S18-O19	σ*	0.16117	3.68	0.96	0.055
-	-	-	S18-O20	σ*	0.15422	3.48	0.97	0.053
-	-	-	S18-O21	σ*	0.33945	3.48	0.75	0.050
C9-C11	π	1.97815	C8-C12	π*	0.33768	26.42	0.28	0.077
-	-	-	C9-C11	π*	0.31517	1.51	0.29	0.019
S18-O19	σ	1.97893	C8- S18	σ*	0.19132	1.12	1.10	0.033
-	-	-	S18-O21	σ*	0.33945	5.22	0.99	0.070
S18-O20	σ	1.98121	S18-O19	σ*	0.16117	2.59	1.20	0.052
-	-	-	S18- O21	σ*	0.33945	4.33	1.00	0.064
S18-O21	σ	1.97762	S18- O19	σ*	0.16117	3.59	1.03	0.056
-	-	-	S18- O20	σ*	0.15422	3.05	1.04	0.052
-	-	-	S18- O21	σ*	0.33945	2.28	0.83	0.042
LPC4	σ	1.01179	C5-N15	π*	0.31815	59.97	0.13	0.095
-	-	-	C9-C11	π*	0.31517	57.88	0.15	0.102
LPN15	σ	1.90438	C3-C4	σ*	0.03973	10.48	0.88	0.087
-	-	-	C4-C9	σ*	0.04215	2.24	0.86	0.040
LPO16	σ	1.97656	C4-C9	σ*	0.04215	6.87	1.09	0.078
LPO16	π	1.82320	C9-C11	π*	0.31517	37.04	0.34	0.104
LPO19	π	1.80959	C8-S18	σ*	0.19132	14.04	0.44	0.071
-	-	-	S18-O20	σ*	0.15422	17.05	0.55	0.087

LPO19	n	1.77962	S18-O20	σ*	0.15422	3.65	0.55	0.041
-	-	-	S18-O21	σ*	0.33945	32.43	0.34	0.096
LPO20	σ	1.98132	C8-S18	σ*	0.19132	1.02	0.95	0.029
LPO20	π	1.80504	C8-S18	σ*	0.19132	14.33	0.44	0.071
-	-	-	S18-O19	σ*	0.16117	17.33	0.54	0.087
LPO20	n	1.77118	C8-S18	σ*	0.19132	3.33	0.44	0.035
-	-	-	S18-O21	σ*	0.33945	33.66	0.33	0.097
LPO21	σ	1.97666	S18-O19	σ*	0.16117	1.67	0.95	0.037
LPO21	π	1.93974	S18-O19	σ*	0.16117	4.12	0.60	0.046
-	-	-	S18-O20	σ*	0.15422	7.99	0.61	0.064

[a]E(2) means energy of hyper-conjugative interactions (stabilization energy in kJ/mol)

[b]Energy difference (a.u) between donor and acceptor i and j NBO orbitals

[c]F(i,j) is the Fock matrix elements (a.u) between i and j NBO orbitals

Table 4. NBO results showing the formation of Lewis and non-Lewis orbitals

Bond (A–B)	ED/e[a]	EDA%	EDB%	NBO	s(%)	p(%)
σC3-C4	1.96717	50.79	49.21	0.7126($sp^{2.14}$)C+	31.86	68.10
-	-0.70894	-	-	0.7015($sp^{1.71}$)C	36.87	63.09
σC4-C9	1.97627	50.86	49.14	0.7132($sp^{2.02}$)C+	33.07	66.88
-	-0.70936	-	-	0.7010($sp^{1.84}$)C	35.20	64.75
πC5-N15	1.79196	40.52	59.48	0.6365($sp^{1.00}$)C+	0.00	100.0
-	-0.32805	-	-	0.7713($sp^{1.00}$)N	0.00	100.0
σC8-S18	1.96254	53.17	46.83	0.7292($sp^{3.21}$)C+	23.72	76.23
-	-0.71371	-	-	0.6843($sp^{2.61)}$S	27.32	71.25
πC9-C11	1.66703	44.66	55.34	0.6683($sp^{1.00}$)C+	0.00	100.0
-	-0.27723	-	-	0.7439($sp^{1.00}$)C	0.00	100.0
σS18-O19	1.97893	34.47	65.53	0.5871($sp^{2.59}$)S+	27.39	71.07
-	-0.94805	-	-	0.8095($sp^{3.44}$)O	22.41	77.16
σS18-O20	1.98121	34.44	65.56	0.5868($sp^{2.57}$)S+	27.62	70.90
-	-0.95611	-	-	0.8097($sp^{3.33}$)O	22.98	76.57
σS18-O21	1.97762	30.01	69.99	0.5479($sp^{4.46}$)S+	17.90	79.89
-	-0.78639	-	-	0.8366($sp^{4.59}$)O	17.86	82.05
n1C4	1.01179	-	-	$sp^{1.00}$	0.00	100.0
-	-0.13690	-	-	-	-	-
n1N15	1.90438	-	-	$sp^{2.63}$	27.51	72.37
-	-0.37184	-	-	-	-	-
n1O16	1.97656	-	-	$sp^{1.32}$	43.12	56.82
-	-0.59938	-	-	-	-	-
n2O16	1.82320	-	-	$sp^{1.00}$	0.00	100.0
-	-0.32721	-	-	-	-	-
n2O19	1.80959	-	-	$sp^{99.99}$	0.12	99.88
-	-0.29636	-	-	-	-	-
n3O19	1.77962	-	-	$sp^{1.00}$	0.00	100.0
-	-0.29587	-	-	-	-	-
n1O20	1.98132	-	-	$sp^{0.30}$	76.87	23.11

-	-0.80442	-	-	-	-	-
n2O20	1.80504	-	-	$sp^{99.99}$	0.10	99.90
-	-0.29518	-	-	-	-	-
n3O20	1.77118	-	-	$sp^{99.99}$	0.03	99.97
-	-0.29371	-	-	-	-	-
n1O21	1.97666	-	-	$sp^{0.69}$	58.96	40.97
-	-0.70340	-	-	-	-	-
n2O21	1.93974	-	-	$sp^{99.99}$	0.19	99.71
-	-0.35274	-	-	-	-	-

[a] ED/e is expressed in a.u.

Table 5

PASS prediction for the activity spectrum of the title compound (Pa represents probability to be active and Pi represents probability to be inactive).

Pa	Pi	Activity
0.979	0.000	Rhamnulose-1-phosphate aldolase inhibitor
0.975	0.001	Glyceryl-ether monooxygenase inhibitor
0.974	0.001	Monodehydroascorbate reductase (NADH) inhibitor
0.973	0.001	Arylacetonitrilase inhibitor
0.972	0.002	Antiseptic
0.966	0.000	(S)-3-hydroxyacid ester dehydrogenase inhibitor
0.965	0.002	Antiprotozoal (Amoeba)
0.960	0.001	Phosphoglycerate mutase inhibitor
0.959	0.001	4-Methoxybenzoate monooxygenase (O-demethylating) inhibitor
0.958	0.001	Glycosylphosphatidylinositol phospholipase D inhibitor
0.955	0.000	Nicotine dehydrogenase inhibitor
0.949	0.001	Gamma-guanidinobutyraldehyde dehydrogenase inhibitor
0.946	0.001	Venom exonuclease inhibitor
0.944	0.001	2-Hydroxyquinoline 8-monooxygenase inhibitor
0.940	0.001	(S)-6-hydroxynicotine oxidase inhibitor
0.936	0.001	Cystathionine gamma-lyase inhibitor
0.938	0.004	Mucomembranous protector
0.934	0.002	IgA-specific metalloendopeptidase inhibitor
0.926	0.002	2-Nitropropane dioxygenase inhibitor
0.925	0.001	Ferredoxin hydrogenase inhibitor
0.923	0.001	Porphobilinogen synthase inhibitor
0.924	0.003	Superoxide dismutase inhibitor
0.921	0.001	2,5-Dihydroxypyridine 5,6-dioxygenase inhibitor
0.921	0.001	Indanol dehydrogenase inhibitor
0.919	0.002	Peroxidase inhibitor
0.914	0.002	Catechol 2,3-dioxygenase inhibitor

Table 6

The binding affinity values of different poses of the title compound predicted by AutodockVina.

Mode	Affinity (kcal/mol)	Distance from best mode (Å)	
-	-	RMSD l.b.	RMSD u.b.
1.	-6.0	0.000	0.000
2.	-5.8	2.761	4.697
3.	-5.5	1.390	3.310
4.	-5.4	2.704	4.713
5.	-5.4	2.429	4.345
6.	-5.3	2.410	3.018
7.	-5.2	2.225	3.138
8.	-4.9	2.557	3.992
9.	-4.6	2.172	2.840

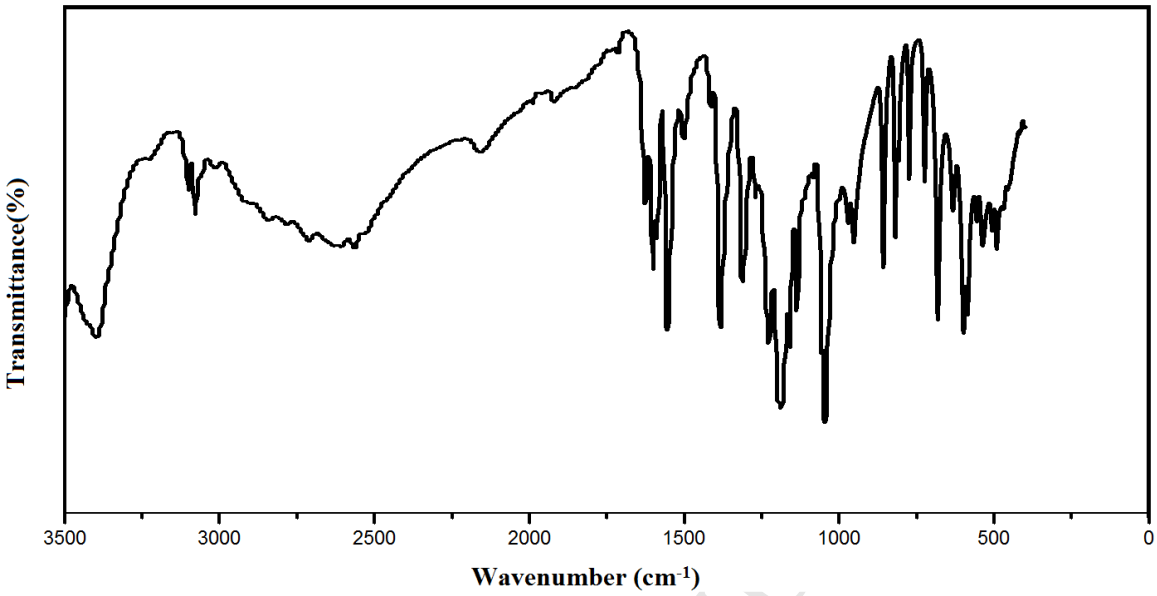

Fig.1 FT-IR spectrum of 8HQ5SA

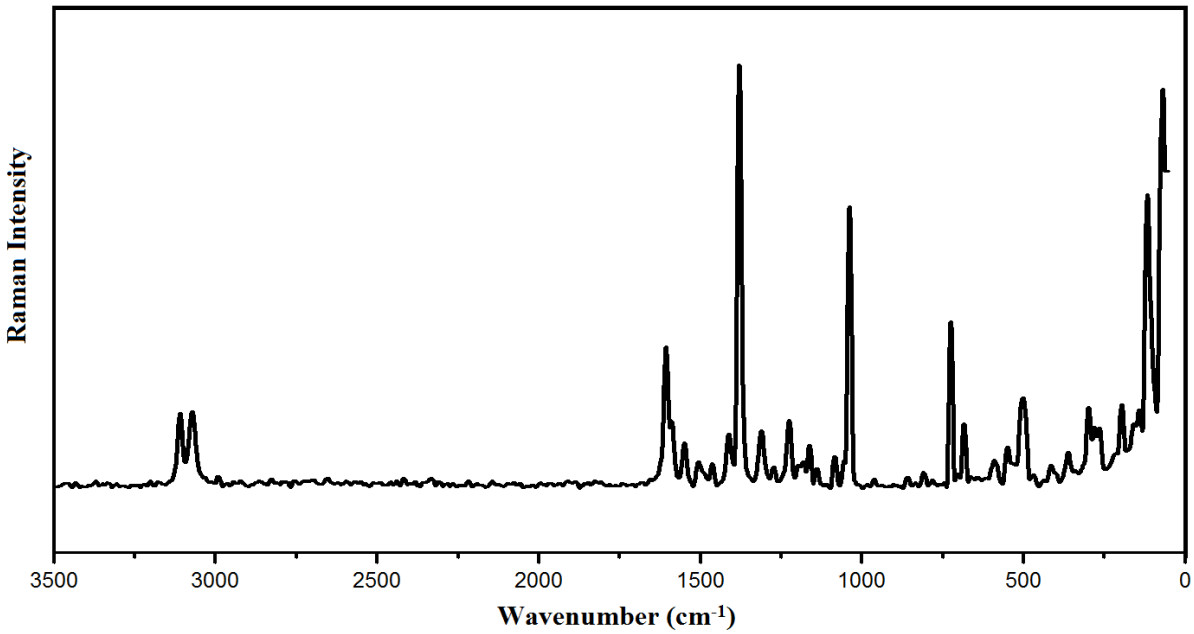

Fig.2 FT-Raman spectrum of 8HQ5SA

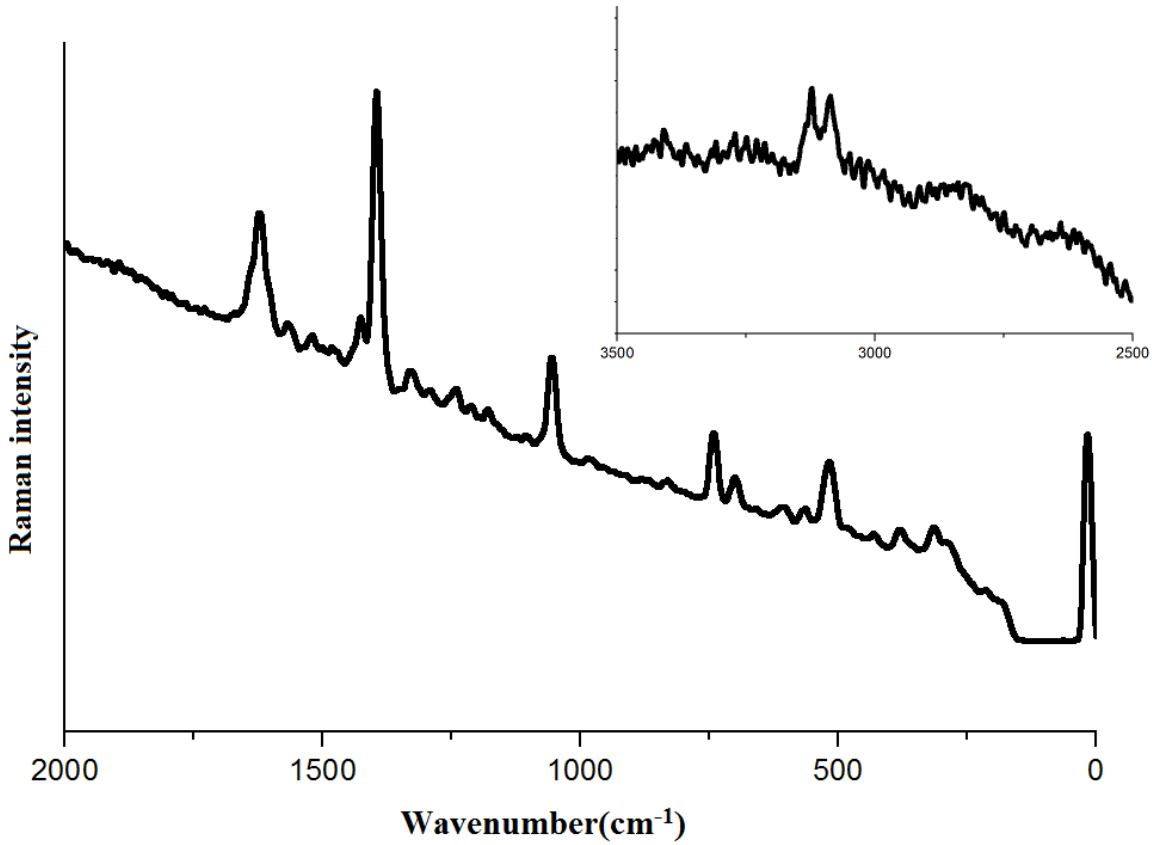

Fig.3 SERS spectrum of 8HQ5SA

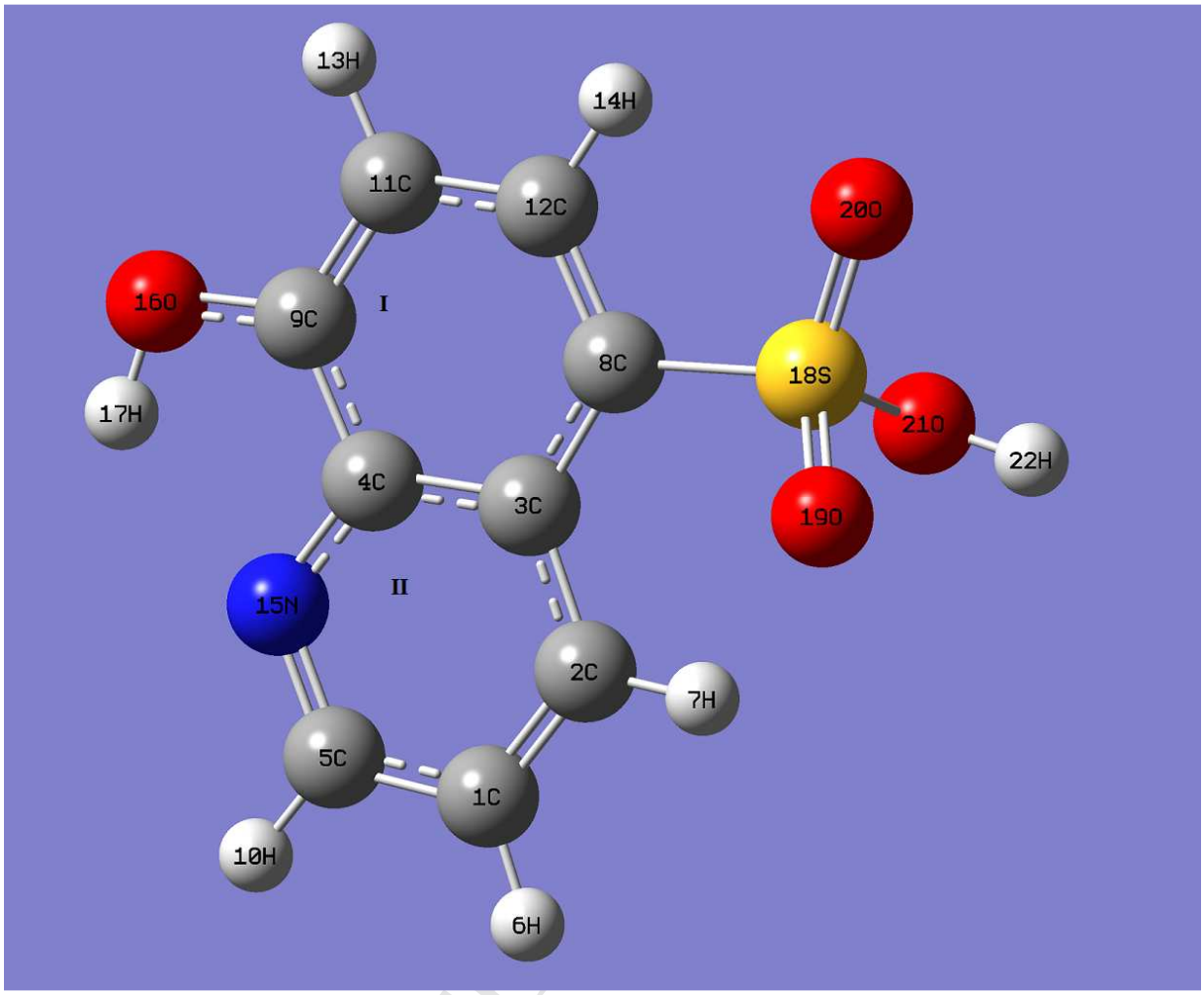

Fig.4 Optimized geometry of 8HQ5SA

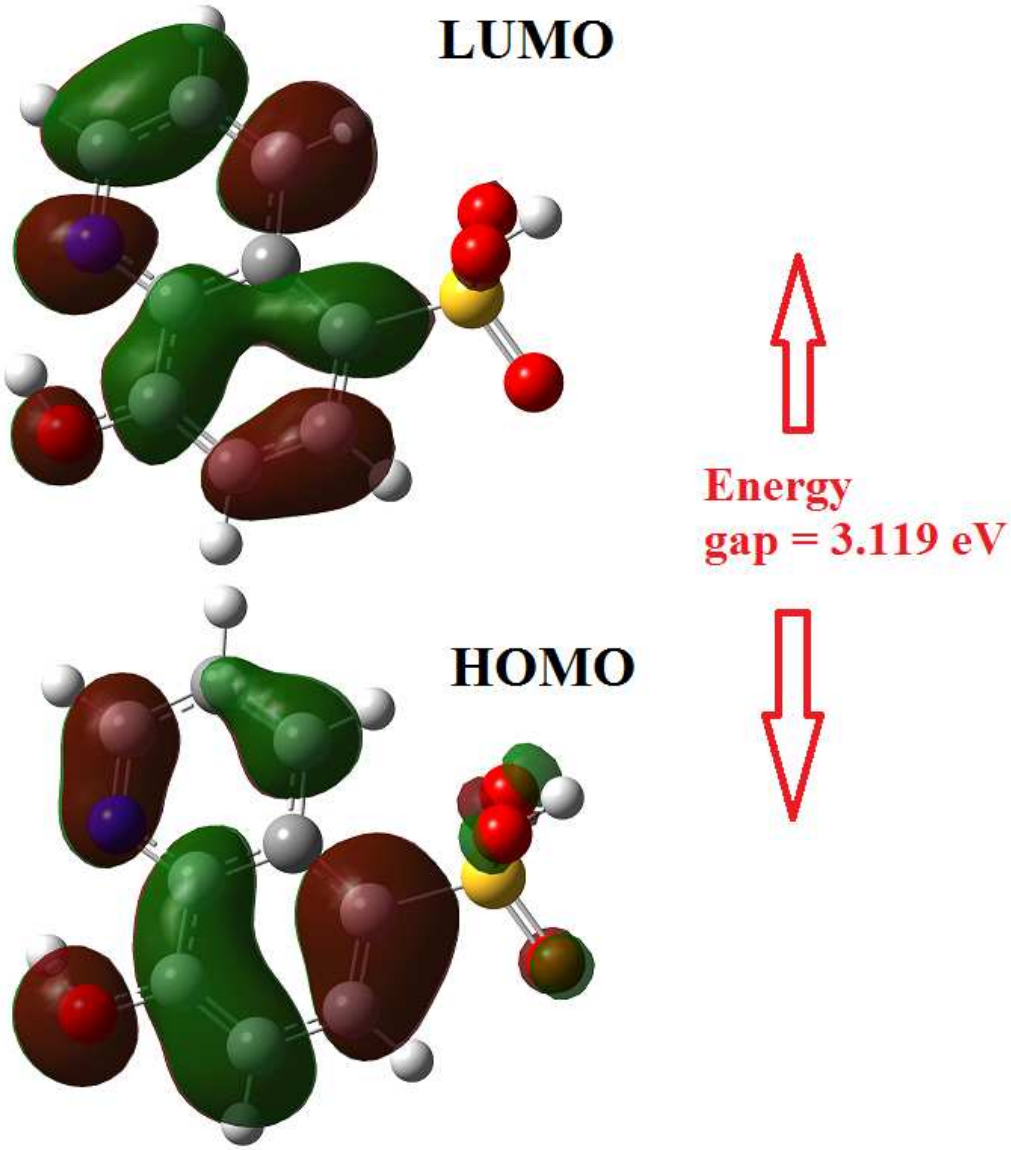

Fig.5 HOMO-LUMO plots of 8HQ5SA

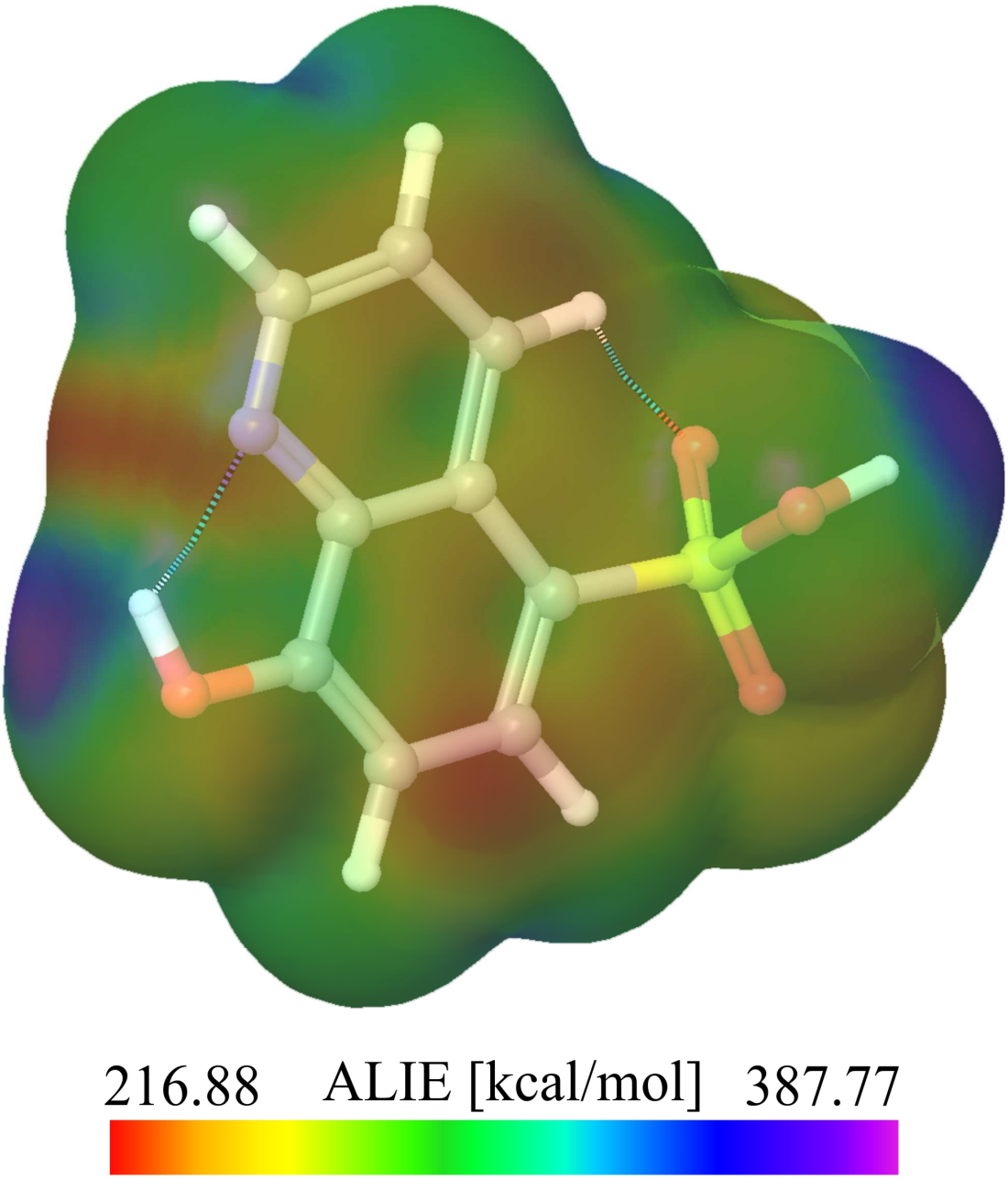

Fig.6 ALIE surface of 8HQ5SA molecule

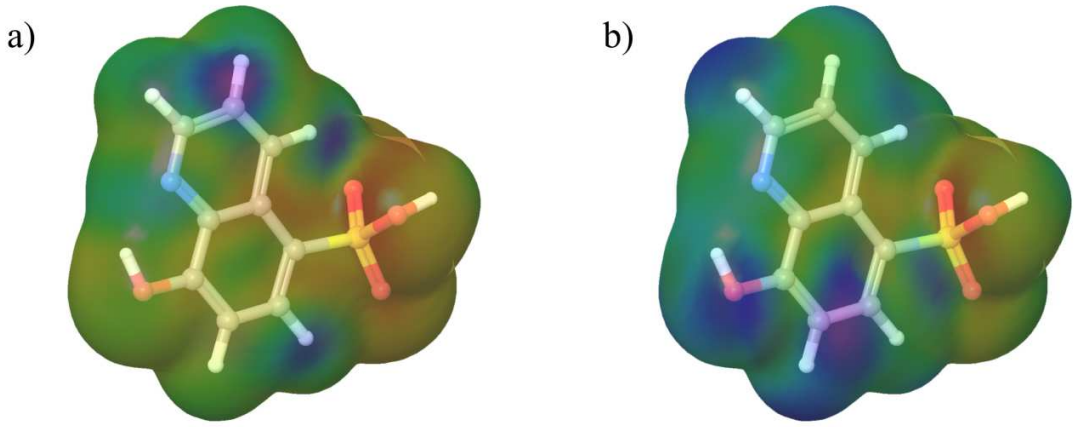

Fig.7 Fukui functions a) f^{+} and b) f^{-} of the 8HQ5SA molecule

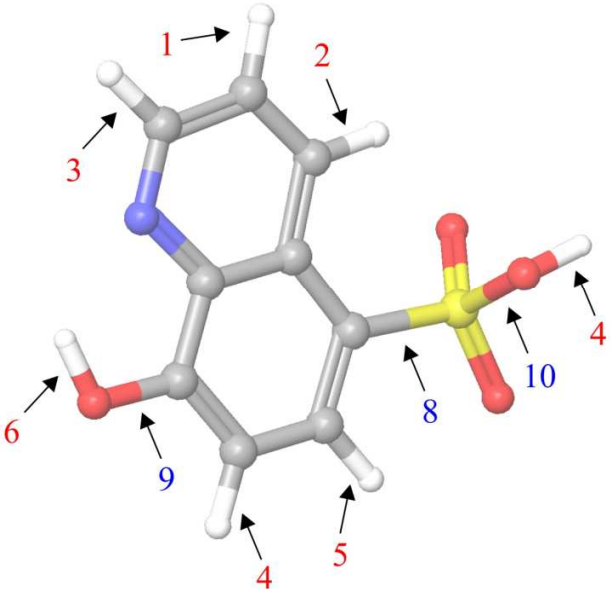

Bond	BDE [kcal/mol]
1	119.15
2	118.10
3	113.25
4	121.24
5	119.36
6	118.55
7	104.96
8	78.24
9	122.87
10	73.80

Fig.8 BDEs of all single acyclic bonds of 8HQ5SA molecule

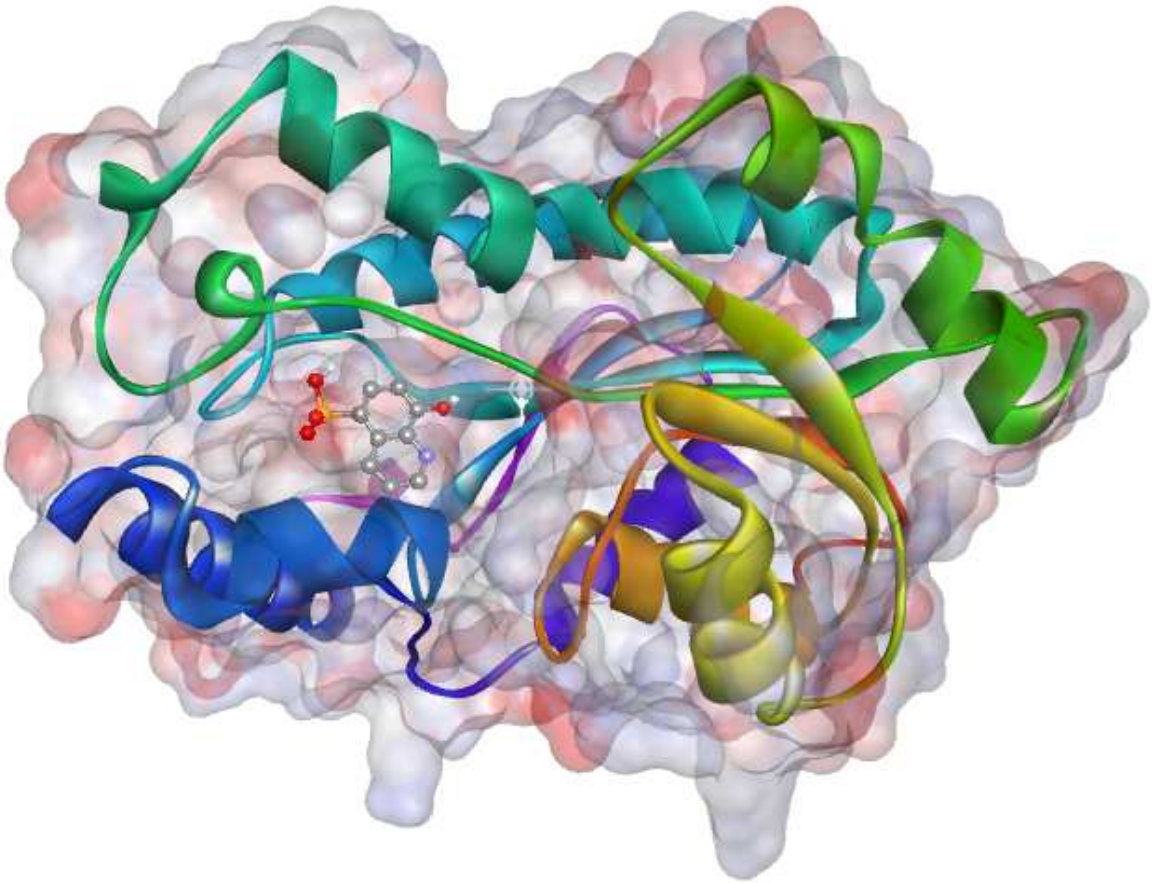

Fig.9 Surface view of the docked ligand embedded in the catalytic site of NADH inhibitor

Highlights

* IR, Raman and SERS spectra were analyzed
* Most reactive sites are identified
* ALIE, BDE, RDF have been discussed in detail
* Docked ligand forms a stable complex with NADH inhibitor.